



Transneuronal Dpr12/DIP- δ interactions facilitate compartmentalized dopaminergic innervation of *Drosophila* mushroom body axons

Bavat Bornstein¹, Hagar Meltzer^{1,*} , Ruth Adler¹, Idan Alyagor¹, Victoria Berkun¹, Gideon Cummings¹, Fabienne Reh², Hadas Keren-Shaul^{3,4}, Eyal David³, Thomas Riemensperger² & Oren Schuldiner^{1,**} 

Abstract

The mechanisms controlling wiring of neuronal networks are not completely understood. The stereotypic architecture of the *Drosophila* mushroom body (MB) offers a unique system to study circuit assembly. The adult medial MB γ -lobe is comprised of a long bundle of axons that wire with specific modulatory and output neurons in a tiled manner, defining five distinct zones. We found that the immunoglobulin superfamily protein Dpr12 is cell-autonomously required in γ -neurons for their developmental regrowth into the distal γ 4/5 zones, where both Dpr12 and its interacting protein, DIP- δ , are enriched. DIP- δ functions in a subset of dopaminergic neurons that wire with γ -neurons within the γ 4/5 zone. During metamorphosis, these dopaminergic projections arrive to the γ 4/5 zone prior to γ -axons, suggesting that γ -axons extend through a prepatterned region. Thus, Dpr12/DIP- δ transneuronal interaction is required for γ 4/5 zone formation. Our study sheds light onto molecular and cellular mechanisms underlying circuit formation within subcellular resolution.

Keywords circuit formation; dopaminergic neurons; IgSF; mushroom body compartments; neuronal remodeling

Subject Category Neuroscience

DOI 10.15252/emj.2020105763 | Received 27 May 2020 | Revised 11 February 2021 | Accepted 19 February 2021 | Published online 13 April 2021

The EMBO Journal (2021) 40: e105763

Introduction

The precise connectivity between neurons is crucial for the function of neural circuits in vertebrates and invertebrates. The formation of neural circuits is especially complex as it is a multi-step process that involves guidance of axons and dendrites belonging to distinct neurons, as well as the identification of subcellular zones on the

target cell onto which synapses are formed. Despite its fundamental nature, our knowledge of the molecular and cellular mechanisms underlying development of neural circuits remains incomplete.

Given its well-studied development, connectivity, and function, the *Drosophila* mushroom body (MB) offers an attractive model to study the mechanisms of neuronal circuit formation and maturation. The MB complex, which functions as a center for associative learning and memory (Heisenberg, 2003; Gerber *et al*, 2004; Fiala, 2007; Oswald & Waddell, 2015; Modi *et al*, 2020), is comprised of both intrinsic and extrinsic neurons (Tanaka *et al*, 2008; Aso *et al*, 2014a). The intrinsic MB neurons are derived from four identical neuroblasts which sequentially give rise to three major classes of unipolar neurons: γ , α'/β' , and α/β , which are collectively known as Kenyon cells (KCs). Axons from each KC type bundle together to form five MB lobes in the adult brain—the vertical α and α' lobes, and the medial γ , β , and β' lobes (Fig 1Q, Crittenden *et al*, 1998). KCs form well-defined circuits with extrinsic MB neurons, including MB output neurons (MBONs) that relay sensory information to higher brain regions, as well as modulatory neurons, which are mostly dopaminergic (DANs). The adult MB KC lobes are innervated by typical MBONs of 22 types (and additionally newly discovered atypical MBON types; Li *et al*, 2020) and by over 150 DANs of 20 types which are divided into two major clusters: protocerebral posterior lateral 1 (PPL1) and protocerebral anterior medial (PAM; Aso *et al*, 2014a). The processes of MBONs and DANs innervate the intrinsic KCs at distinct and stereotypic locations along the MB lobes, thereby defining discrete zones, also known as compartments, within the lobes (due to a potential confusion between cell intrinsic compartments such as the axon initial segment, here we use the term zone to describe these lobe compartments; Tanaka *et al*, 2008; Aso *et al*, 2014a). In the case of the adult γ -lobe, which is comprised of intrinsic γ -KC axons, stereotypic innervations by DANs and MBONs define five distinct axonal zones, termed γ 1- γ 5 (see scheme in Fig 1Q as well as models in Fig 1P and Movie EV1 which are both based on EM traces [Scheffer *et al*, 2020]; see

1 Department of Molecular Cell Biology, Weizmann Institute of Science, Rehovot, Israel

2 Institute of Zoology, University of Cologne, Köln, Germany

3 Department of Immunology, Weizmann Institute of Science, Rehovot, Israel

4 Life Science Core Facility, Weizmann Institute of Science, Rehovot, Israel

*Corresponding author. Tel: +972 8 9342775; E-mail: hagar.meltzer@weizmann.ac.il

**Corresponding author (lead contact). Tel: +972 8 9342769; E-mail: oren.schuldiner@weizmann.ac.il

methods for more details). Interestingly, recent analyses of EM data suggest further categorization of the PAM-DANs innervating the γ_5 zone into five anatomically distinct subtypes, suggested to perform different functions (Otto *et al.*, 2020). Each γ -KC axon extends throughout the entire lobe and forms synaptic boutons with the dendrites of distinct MBONs and processes of DANs within each zone. Remarkably, a recent study has shown that boutons within the same KC, but in different zones, often exhibit distinct calcium dynamics (Bilz *et al.*, 2020). Finally, these zones have distinct functional roles; DANs innervating the γ_1 - γ_2 zones are associated with aversive memory, while DANs innervating the γ_4 - γ_5 zones promote appetitive memory (Aso *et al.*, 2014a; Cohn *et al.*, 2015; Cognigni *et al.*, 2018). Despite their functional importance, the cellular and molecular mechanisms that control MB circuit and zone formation are not known.

The MB is attractive to study wiring of neural circuits not only due to its complex yet stereotypic nature, but also due to its multi-step development. The larval MB is primarily comprised of γ -KCs, which form two axonal lobes (vertical and medial γ -lobes). While larval and adult MB lobes follow the same basic organizational principles in which DANs and MBONs define distinct zones, the actual zonation pattern differs between these two developmental stages (Rohwedder *et al.*, 2016; Saumweber *et al.*, 2018). The larval γ -lobes undergo extensive remodeling during metamorphosis, including axon pruning followed by developmental regrowth (Lee *et al.*, 1999; Fig 1A), to give rise to the adult medial γ -lobe containing the γ_1 - γ_5 zones (Fig 1Q). We have previously demonstrated that regrowth of the adult γ -lobe is genetically controlled by the nuclear receptor Unfulfilled (UNF) functioning as a ligand-dependent transcription factor, by mechanisms distinct from initial axon outgrowth (Yaniv *et al.*, 2012). Importantly, while we found that UNF promotes axon regrowth partly via the TOR pathway, it is yet unclear through which mechanisms it promotes targeting, circuitry, and sub-zone formation. Here, we exploit detailed expression profile analyses to focus on the Immunoglobulin superfamily (IgSF) proteins as potential mediators of zone formation and circuit wiring within the $\gamma_4/5$ zones.

Results

Dpr12 is required for the full regrowth of γ -KCs

To identify potential genes and pathways that mediate axon regrowth and circuit formation, we sequenced the RNA content of WT γ -KCs during development (Alyagor *et al.*, 2018) alongside γ -KCs expressing RNAi targeting UNF, a known protein required for regrowth (Fig 1A). Dataset EV1 shows this comparison alongside the previously generated (Alyagor *et al.*, 2018) expression profiles of γ -KCs expressing a dominant-negative form of the ecdysone receptor (Ecr^{DN}), which is required for pruning (Lee *et al.*, 2000; data are freely available in: <https://www.weizmann.ac.il/mcb/Schuldiner/re-sources>). The immunoglobulin superfamily (IgSF) appeared as the protein family most significantly affected by UNF-RNAi expression ($P = 3 \times 10^{-29}$; analyzed in <http://www.flymine.org/>). Within the IgSF, the defective proboscis response (Dpr) family stood out as 16 of 21 members were significantly expressed in dynamic patterns in developing γ -KCs (Fig 1B, Dataset EV2). We found that the

transcription of approximately half of the Dprs (7/16; Dataset EV2) was significantly reduced in UNF-RNAi-expressing flies. Interestingly, the interactions between the Dprs, containing two immunoglobulin (Ig) domains, and the Dpr-interacting proteins (DIPs), containing three Ig domains, are important for proper development and synaptic connectivity of the *Drosophila* visual system and neuromuscular junction (NMJ; Xu *et al.*, 2018; Ashley *et al.*, 2019; Venkatasubramanian *et al.*, 2019). Based on these data, we focused on the Dprs as potential candidates required for regrowth and circuit reformation.

We targeted eight different Dprs in γ -KCs by RNAi (Fig EV1A) based on reagent availability (TRIP lines, <https://fgr.hms.harvard.edu/fly-in-vivo-rnai>), using a γ -specific driver (R71G10, which is predominantly and consistently expressed in γ -KCs, but is also expressed in α/β -KCs in a stochastic manner; see Appendix Table S2). Seven of these RNAis did not affect γ -neuron development. While it is possible that these Dprs are indeed not required for γ -KC development, the lack of phenotype may also result from inherent redundancies of Dpr-DIP interactions (Cosmanescu *et al.*, 2018), or, alternatively, from limited efficiency of the RNAi lines. In contrast, expressing *dpr12* RNAi in γ -KCs induced a pronounced regrowth defect, where axons did not occupy the distal portion of the γ -lobe (Figs 1C and D, and EV1A). Interestingly, the expression of *Dpr12* is markedly reduced in neurons expressing UNF-RNAi at the relevant times for regrowth (Figs 1B, and EV1A, Dataset EV2), suggesting that UNF might positively regulate *dpr12* transcription. These findings suggest that Dpr12 could promote developmental regrowth and circuit formation as a part of an UNF-dependent transcriptional program.

To validate the RNAi results, we next perturbed Dpr12 through tissue-specific (ts)CRISPR using Gal4-driven Cas9 expression (Port & Bullock, 2016; Meltzer *et al.*, 2019; Port *et al.*, 2020). tsCRISPR of *dpr12* in γ -KCs induced a defect closely resembling the RNAi phenotype (Fig 1E and F). Finally, we used CRISPR/Cas9 technology to generate a *dpr12* loss-of-function mutant (*dpr12* ^{$\Delta 50-81$} , Fig EV1B and C). At 3rd instar larva (L3), γ -KCs in *dpr12* ^{$\Delta 50-81$} homozygotes exhibited WT morphology (Fig 1G and K) and subsequently pruned normally (as evident by the lack of unpruned axons in the adult, Fig 1L and M). These data indicate that Dpr12 is not required for initial axon extension or pruning. In contrast, γ -KCs in *dpr12* ^{$\Delta 50-81$} animals failed to extend to the distal part of the lobe during the mid-pupal stage (at 48 h APF), a time when γ -axons would have normally completed their regrowth (Lee *et al.*, 1999; Rabinovich *et al.*, 2016), and in the adult (Fig 1H,I,L,M,O). Importantly, γ -specific expression of a *Dpr12* transgene significantly rescued the regrowth defect within *dpr12* ^{$\Delta 50-81$} homozygotes (Fig 1J,N,O, ranking examples shown in Fig EV1D). Together, these data demonstrate that Dpr12 is required for full axon regrowth during metamorphosis and that mutant γ -axons stop prematurely and do not extend into the distal end of the lobe. Importantly, its requirement during metamorphosis does not rule out additional roles of Dpr12 in other developmental stages.

Dpr12 is cell-autonomously required for γ -axon regrowth into the $\gamma_4/5$ zones

To determine whether Dpr12 functions in a cell-autonomous manner, we used the mosaic analysis with a repressible cell marker (MARCM) technique to express *dpr12*-RNAi within neuroblast (NB)

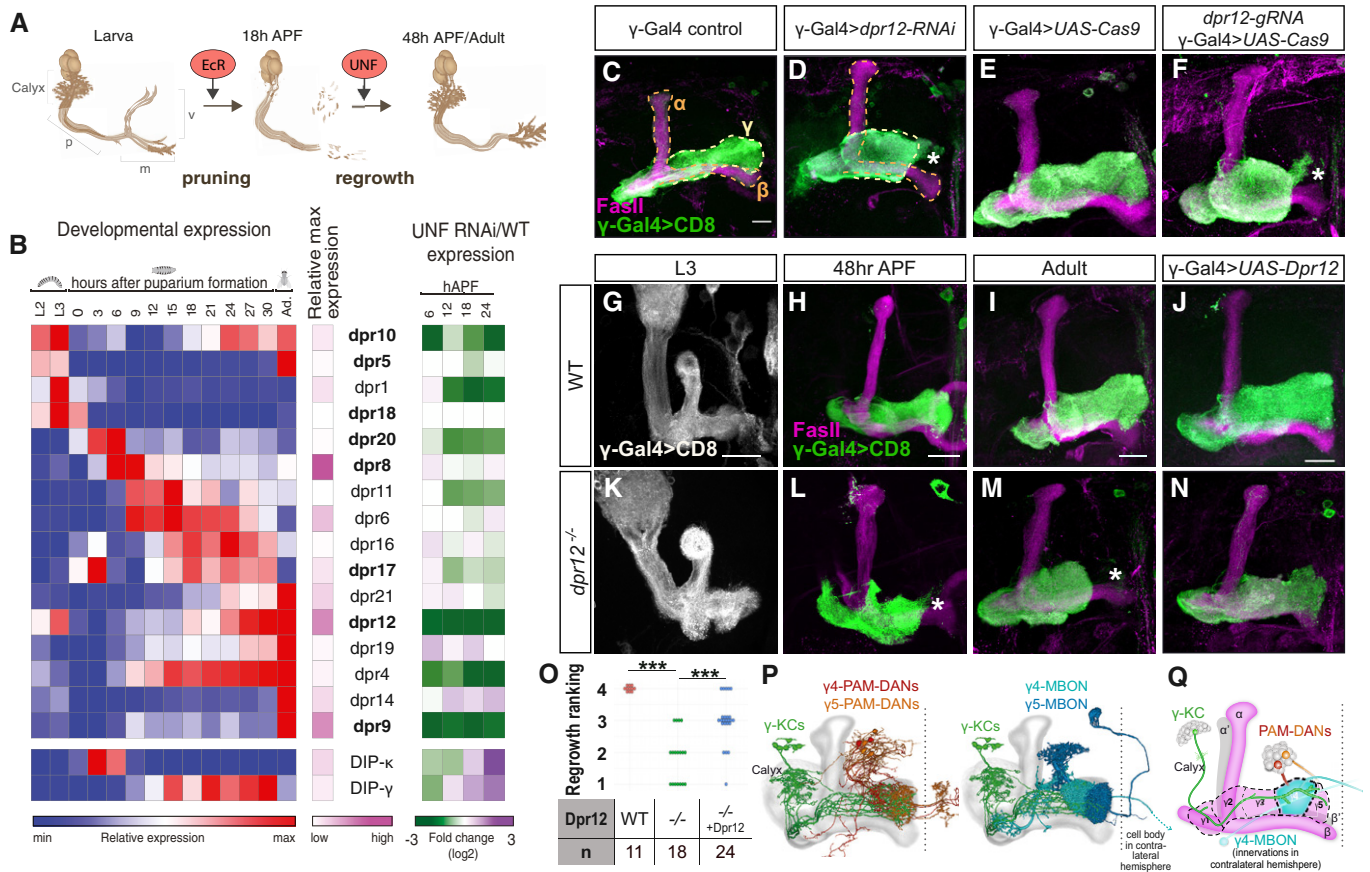


Figure 1. Dpr12 is required for full extension of γ -KCs.

- A Schematic representation of neuronal remodeling of γ -KCs and its regulation by the nuclear receptors ECR and UNF. p: axon peduncle; m/v: medial and vertical lobes.
- B Dynamic expression of Dprs and DIPs during γ -KC development. Left: Heatmap depicting the relative expression patterns of Dprs and DIPs in γ -KCs during development. Middle: Magenta intensity depicts the peak expression of each gene during development relative to other Dprs and DIPs. Right: Expression change of Dprs and DIPs while knocking down the UNF transcription factor compared to WT γ -KCs. Dprs highlighted in bold were tested in the RNAi mini-screen (Fig EV1).
- C–N Confocal z-projections of the indicated genotypes and age, labeled with membrane-bound GFP (mCD8-GFP; CD8) driven by the γ -specific Gal4 driver GMR71G10-Gal4 (γ -Gal4). While γ -axons of control flies project through the entire lobe (C is the RNAi control; $n = 12/12$, E is the tsCRISPR control; $n = 14/14$), knockdown of *dpr12* by RNAi (D; $n = 12/12$) or knockout by tsCRISPR (F; $n = 14/14$) resulted in short axons. At L3, γ -axons in *dpr12* ^{Δ 50-81} homozygote mutant animals (K; $n = 20/20$) resemble WT γ -axons (G; $n = 20/20$). At 48 h APF, WT γ -axons normally re-extend to form the adult lobe (H; $n = 12/12$). *dpr12* ^{Δ 50-81} γ -axons (L; $n = 14/14$) fail to extend to the end of the lobe. This defect persists to adult (I; $n = 11/11$ vs. M; $n = 18/18$). Expressing a *UAS-Dpr12* transgene within γ -KCs in *dpr12* ^{Δ 50-81} homozygote mutant animals rescued the axon regrowth defect (N; $n = 23/24$, J; $n = 14/14$). The adult γ -lobe and α/β lobes are outlined in (C, D) in yellow and orange, respectively, for clarity. Asterisks demarcate the distal part of the lobe. Green and white indicate mCD8-GFP. Magenta represents FasII staining. Scale bar is 20 μ m.
- O Quantification of the regrowth defects in (I, M, and N). The z-projections were blindly classified into four classes of regrowth defect severity; see Fig EV1D for examples. Significance was calculated by Kruskal–Wallis test followed by a Mann–Whitney post hoc test; *** $P < 0.001$.
- P Models based on hemibrain EM traces (Scheffer et al, 2020) of adult γ -KCs (representative neurons shown in green), in relation to either selected PAM-DANs (left; red and orange) or MBONs (right; cyan and blue) targeting the γ 4 and γ 5 zones. Note that the cell body of the γ 4-MBON is located in the contralateral hemisphere. The MB neuropil is shown in gray. See Materials and Methods for additional details.
- Q Schematic representation of the adult MB. The bundled γ -KCs form the γ -lobe (an example of a single γ -KC is depicted in green). The γ 1– γ 5 zones are defined by stereotyped and tiled innervations of the γ -lobe by dopaminergic neurons (DANs; examples of DANs targeting the γ 4 and γ 5 zones are depicted in red and orange, respectively) and MB output neurons (MBONs; an example of the γ 4 > γ 1 γ 2 MBON innervation is shown in cyan to match the schematics in Fig 7E and F; note that its cell body and innervations are located in contralateral hemispheres). Black dashed line represents the midline. Magenta represents typical FasII staining (which stains the α/β' lobes and the γ -lobe but not the α'/β' lobes).

or single-cell (SC) clones. We found that both NB and SC γ -KC clones expressing *dpr12* RNAi exhibited normal growth at L3 but failed to fully extend axons at 48 h APF and in adult flies (Fig 2A–L). Based on these results, we conclude that Dpr12 is cell-autonomously required in γ -KCs for their full developmental regrowth.

Interestingly, unlike other mutants that affect developmental regrowth (Yaniv et al, 2012; Yaniv et al, 2020), *dpr12* mutant axons seem to partially regrow but stop prematurely in a particular and stereotypic location along the lobe. Therefore, and given that the γ -lobe is divided into distinct zones, we next mapped the location of

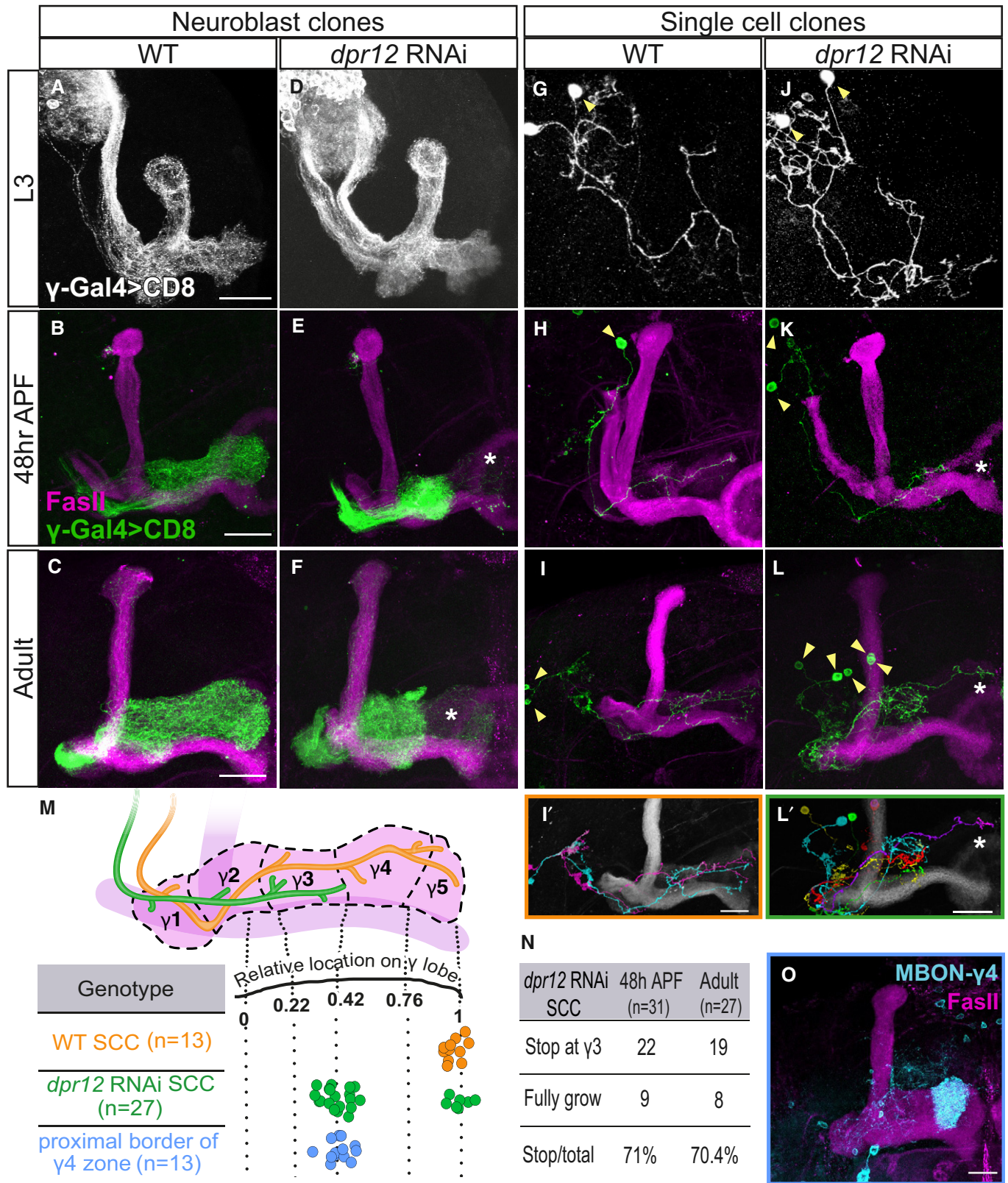


Figure 2.

Figure 2. Dpr12 is cell-autonomously required for γ -axon regrowth into the γ 4/5 zones.

- A–L Confocal z-projections of MARCM neuroblast (NB, A–F) and single-cell (SC, G–L) clones labeled with membrane-bound GFP (mCD8-GFP; CD8) driven by the γ -specific Gal4 driver GMR71G10-Gal4 (γ -Gal4). At L3, NB and SC clones expressing *dpr12* RNAi are similar to equivalent WT clones (A; $n = 20/20$, D; $n = 15/15$, G; $n = 15/15$ and J; $n = 17/17$). At 48 h APF and adult stage, WT NB (B; $n = 15/15$, C; $n = 10/10$) and SC (H; $n = 16/16$, I; $n = 13/13$) clones extend their axons to form the full adult lobe. In contrast, clones expressing *dpr12* RNAi (E; $n = 14/14$, F; $n = 22/2$, K; $n = 18/24$, L; $n = 19/27$) fail to extend their axons to the distal part of the medial lobe (asterisks). (I' and L') are traces of multiple single-cell clones depicting each cell in a different color.
- M Top: Schematic representation of WT (orange) and *dpr12* RNAi-expressing (green) single γ -KC axons. Bottom: Measurements of the relative location to which WT (I) and *dpr12* RNAi (L) axons grow across the entire length of the adult γ lobe, alongside the relative position of the proximal border of the γ 4 zone (see O, as well as Fig EV2).
- N A table depicting the percentage of *dpr12* RNAi-expressing single-cell clones (SCCs) which stop at the γ 3– γ 4 border, at 48 h APF compared to the adult stage.
- O Confocal z-projection of MBON γ 4 > γ 1 γ 2 labeled by GMR18H09-Gal4 driving the expression of mCD8-GFP (CD8) shown in cyan.
- Data information: Yellow arrowheads demarcate single cell bodies. Green, white, and cyan represent mCD8-GFP. Magenta represents FasII. Scale bar is 20 μ m.

the premature stopping in more detail. We measured the length of adult WT and mutant axons relative to the γ -lobe span and superimposed these data onto the γ -lobe zones (Fig 2M), as defined by distinct innervations of MBONs and DANs (Figs 2O and EV2; Aso et al, 2014a; Shuai et al, 2015). This analysis indicated that the premature stopping of clones expressing *dpr12* RNAi correlates with the border between the γ 3 and γ 4 zones (Fig 2I', L', M, Movies EV2 and EV3). We found that the majority of SC clones stopped at the γ 3/4 border, while only a minority extended to the end of the lobe (Fig 2M). We also observed brains containing multiple single-cell clones, in which one axon extended to the edge of the lobe, while the remaining stopped prematurely, ruling out a brain-specific effect (Fig 2L'). Importantly, the proportion of SCCs that stalled at the γ 3/4 border was similar in both adults and at the earlier developmental stage of 48 h APF (70.4% and 71%, respectively; Fig 2N). Since 48 h APF is the time point in which axons normally complete their regrowth, this suggests that the phenotype observed in the adult stage is the result of arrested regrowth, rather than retraction of previously grown axons. Since axons always stall at a discrete location, our data suggest that the phenotype does not arise from reduced growth potential, *per se*, but rather through a failure to recognize a molecular signal at a designated and stereotypic location (see discussion). Overall, we conclude that Dpr12 is cell-autonomously required for γ -KC projection into the MB γ 4/5 zones.

Dpr12 and its putative interacting protein DIP- δ localize at the γ 4/5 zones

To assess Dpr12 protein localization, we used the *Minos*-mediated integration cassette (MiMIC) transgene collection to obtain a GFP insertion within the endogenous *Dpr12* locus, which should produce a Dpr12-GFP fusion protein (Dpr12^{GFSTF}; Fig EV1B and C; Nagarkar-Jaiswal et al, 2015). We found that Dpr12-GFP localized to the distal part of γ -axons at late larva (L3; Fig 3A), then becoming diffuse at 24 h APF, when γ -axons initiate their developmental regrowth (Fig 3B). Finally, at 48 h APF up until adulthood, Dpr12 relocated to the distal part of the lobe (Fig 3C and D, Appendix Fig S1A) and was highly enriched within the adult γ 4 and γ 5 zones (Fig 3D; Appendix Fig S1E). Our data suggest that Dpr12 is expressed at the right time and place to mediate γ -axon regrowth into the γ 4/5 zones.

Dprs can form heterophilic interactions with DIPs in a rather promiscuous fashion, in which most Dprs can bind to multiple DIPs and most DIPs can bind to multiple Dprs (Ozkan et al, 2013; Carrillo et al, 2015; Cosmanescu et al, 2018). Interestingly, Dpr12 and DIP- δ

represent a unique case of “monogamous” binding. We found that DIP- δ -GFP (DIP- δ ^{GFSTF}; Fig EV3A and B) is also localized to both the γ 4 and γ 5 zones, although its expression is significantly stronger in γ 4 compared to γ 5 (Fig 3G and H; Appendix Fig S1F). In contrast to Dpr12, DIP- δ was localized to the distal MB lobe at all developmental time points tested (Fig 3E–H, Appendix Fig S1B), including at 24 h APF, when γ -axons are completely pruned and have not yet extended (Fig 3F). Transverse sections across the γ 4 zone in the adult stage clearly demonstrate the colocalization of both the Dpr12 and DIP- δ proteins with γ 4 (as determined by the well-characterized MBON γ 4 > γ 1 γ 2; Fig 3D and H). Taken together, these data indicate that DIP- δ is localized to the γ 4/5 zones throughout development and is expressed in cells that project to this region before γ -KCs reach their terminal projections.

DIP- δ is non-cell-autonomously required for full γ -axon regrowth

We next asked whether DIP- δ is also required for the extension of γ -axons into the γ 4/5 zones. We therefore both generated and obtained *DIP- δ* mutant alleles (*DIP- δ ^{T2A-Gal4}*, *DIP- δ ¹⁻¹¹⁹*, respectively; Fig EV3A and B). We marked the γ -KCs by expressing a membrane-bound tomato (QUAS-mtdT-3XHA) driven by the Gal4-independent γ -KC QF2 driver (71G10-QF2; note that, as its Gal4 counterpart, in addition to consistent expression within γ -KCs, 71G10-QF2 is also stochastically expressed in α/β -KCs; see Appendix Table S2). At L3, γ -KCs within *DIP- δ* mutant brains exhibited WT morphology (Figs 4A and E, and EV3C), indicating that DIP- δ is not required for their initial axon extension. However, *DIP- δ* mutant brains displayed a γ -axon regrowth defect at 48 h APF and in adult (Figs 4B, C, F, G, and EV3D), which resembled the *dpr12* mutant phenotype. To confirm that *DIP- δ* loss of function induced this γ -axon regrowth defect, we exploited the fact that the *DIP- δ ^{T2A-Gal4}* allele also expresses Gal4 in DIP- δ ⁺ neurons (Fig EV3A and B). Expressing a *DIP- δ* transgene driven by *DIP- δ ^{T2A-Gal4}* rescued the γ -axon extension defect (Fig 4D, H, I, and EV3E), confirming that DIP- δ is required for γ -axon innervation of the γ 4/5 zones.

To identify these DIP- δ -expressing cells, we expressed DIP- δ RNAi in different cell types, while simultaneously labeling γ -KCs using the QF2 system described above. Driving the expression of *DIP- δ* -RNAi in all glia (using the Pan-glial driver Repo-Gal4) or all KCs (using OK107-Gal4) did not affect γ -axon extension (Fig 4J and K). In contrast, knocking down of *DIP- δ* in all neurons (using the pan-neuronal driver C155-Gal4) or all DIP- δ -expressing neurons (using *DIP- δ ^{T2A-Gal4}*) resulted in stalled γ -axons that do not innervate

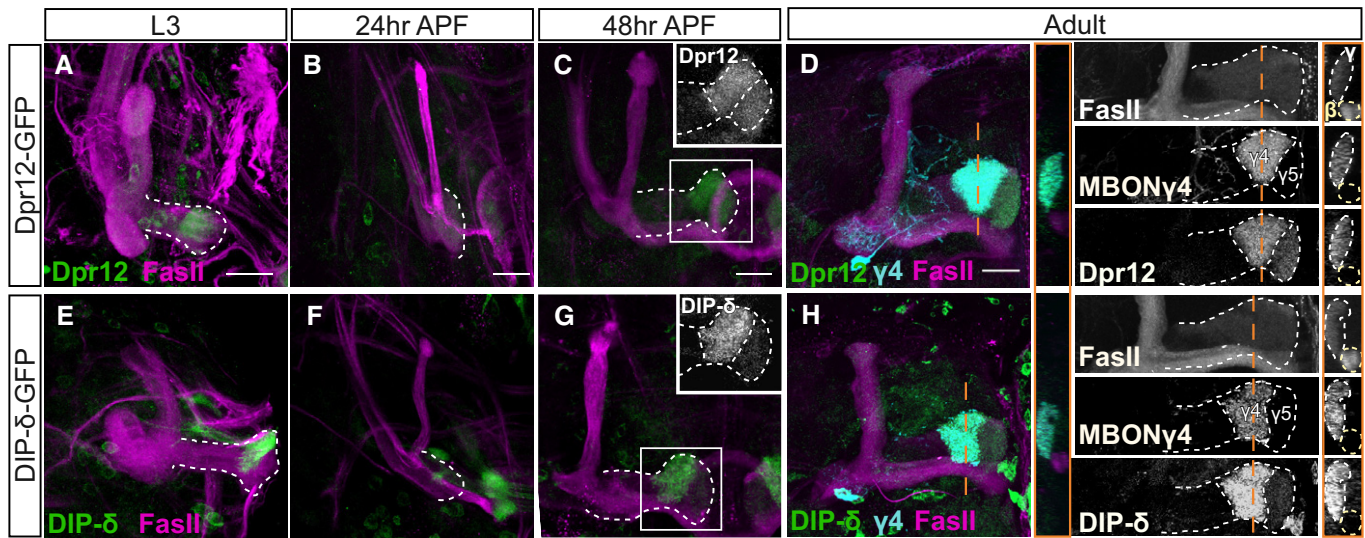


Figure 3. Both Dpr12 and its interacting protein DIP- δ localize to the γ 4/5 zones.

A–H Confocal z-projections of brains expressing MiMIC mediated Dpr12^{GFP} (Dpr12-GFP; A–D) and DIP- δ ^{GFP} (DIP- δ -GFP; E–H) fusion proteins at the indicated time points. See Figs EV1 and EV3 for more details on the fusion protein structure. (A–D) Dpr12-GFP is localized to the distal part of the γ -lobe at L3 (A; $n = 10/10$), 48 h APF (C; $n = 12/12$) and the adult stage (D; $n = 20/20$), where it colocalizes with the γ 4 > γ 1 γ 2 MBON (γ 4; labeled by GMR18H09-Gal4 driving the expression of CD4-tdT). At 24hr APF (B; $n = 10/10$), Dpr12-GFP appears diffuse. (E–H) DIP- δ -GFP is localized to the distal part of the γ -lobe throughout development: L3 (E; $n = 16/16$), 24 h APF (F; $n = 10/10$), 48 h APF (G; $n = 12/12$), and adult (H; $n = 24/24$). At the adult stage, DIP- δ -GFP is colocalized with the γ 4 > γ 1 γ 2 MBON (γ 4).

Data information: White dashed lines depict the γ -lobe. Green is GFP, cyan is CD4-tdT, and magenta is FasII. Grayscale in the right panels of (D and H) represents single channels, as labeled. Insets in (C, G) represent grayscale magnifications of the GFP channel within the white boxes. In orange are transverse sections through the γ 4 zone at the indicated locations; the γ -lobe is outlined in white and the β -lobe in yellow. Scale bar is 20 μ m.

the γ 4/5 zones (Fig 4L and M; Appendix Table S2). Similarly, tsCRISPR of *DIP- δ* in all neurons, but not when restricted to γ -KCs, affected the extension of γ -axons (Fig EV3F–I). Together, these experiments indicate that DIP- δ is not required in γ or other KCs. Rather, DIP- δ likely functions in extrinsic MB neurons in a non-cell-autonomous manner to mediate γ -axon extension into the γ 4/5 zones.

A sub-population of DANs express DIP- δ in the γ 4/ γ 5 zones

Our data suggest that DIP- δ is expressed in extrinsic MB neurons that innervate the γ 4/ γ 5 zones (Figs 3 and 4). These zones are strongly innervated by a sub-population of PAM-DANs, as well as by three typical MBONs: MBON γ 4 > γ 1 γ 2 (also known as MBON-05), MBON γ 4 γ 5 (MBON-21), and MBON γ 5 β '2a (MBON-01; Aso *et al.*, 2014a; Li *et al.*, 2020; Tanaka *et al.*, 2008). To investigate whether DIP- δ is expressed in these cells, we selectively ablated PAM-DANs or MBONs by cell type specific expression of Diphtheria toxin (UAS-DTI) and assayed DIP- δ -GFP localization in adult flies. Ablating one of the two γ 4-MBONs, MBON- γ 4 > γ 1 γ 2, did not affect DIP- δ expression (Fig 5A and B). In contrast, ablating PAM-DANs using R58E02-Gal4 drastically reduced γ 4/5 specific DIP- δ expression (Fig 5C and D). While we cannot exclude the possibility that DIP- δ is additionally expressed in the other γ 4-MBON (MBON- γ 4 γ 5), these results strongly suggest that at the adult stage, DIP- δ protein that is localized to the γ 4/5 zones is mainly, if not exclusively, expressed by PAM-DANs. This finding is consistent with recent profiling experiments which showed that DIP- δ is highly enriched in PAM-DANs (and was in fact even suggested as a new marker for these neurons; Croset *et al.*, 2018).

Next, we wanted to visualize PAM-DANs during development to determine whether they may provide a template for γ -axon growth, as suggested by DIP- δ -GFP expression (Fig 3). However, the “classical” PAM-DAN driver, R58E02, is not expressed throughout development (Fig EV4A–C, Appendix Table S2). We therefore analyzed the expression of *DIP- δ ^{T2A-Gal4}* and found that it is widespread throughout development. While it is expressed in cells innervating the γ 4–5 zones (Fig EV4E and F), it is also, for example, expressed in cells that send processes to the MB vertical lobes. We thus decided to use the MARCM technique to label sparse *DIP- δ ^{T2A-Gal4}* clones (Fig 5E–G; of note, these clones remain heterozygous for DIP- δ). We detected DIP- δ -expressing clones that innervate the γ 4/ γ 5 zones as early as 24 h APF and up to adulthood. Interestingly, these clones do not seem to express tyrosine hydroxylase (TH), required for Dopamine biogenesis, at 24 h APF but become TH positive at 48 h APF onwards. Notably, while DIP- δ -expressing PAM-DANs innervate both the γ 4 and γ 5 zones, their innervation of γ 5 is sparser than that of γ 4 (Fig 5G). This correlates with the reduced enrichment of the DIP- δ protein in γ 4 compared to γ 5 (Fig 3G and H). In summary, our data suggest that DIP- δ is expressed in PAM-DANs, which innervate the future γ 4/5 zones as early as 24 h APF, and support the speculation that DIP- δ expressed in PAM-DANs may provide a template for γ -axon growth.

DIP- δ is required and sufficient for Dpr12 localization

Both Dpr12 and DIP- δ localize to the γ 4/5 zones and are required for their formation likely by mediating interactions between the γ -KCs and the PAM-DANs. We therefore investigated how losing

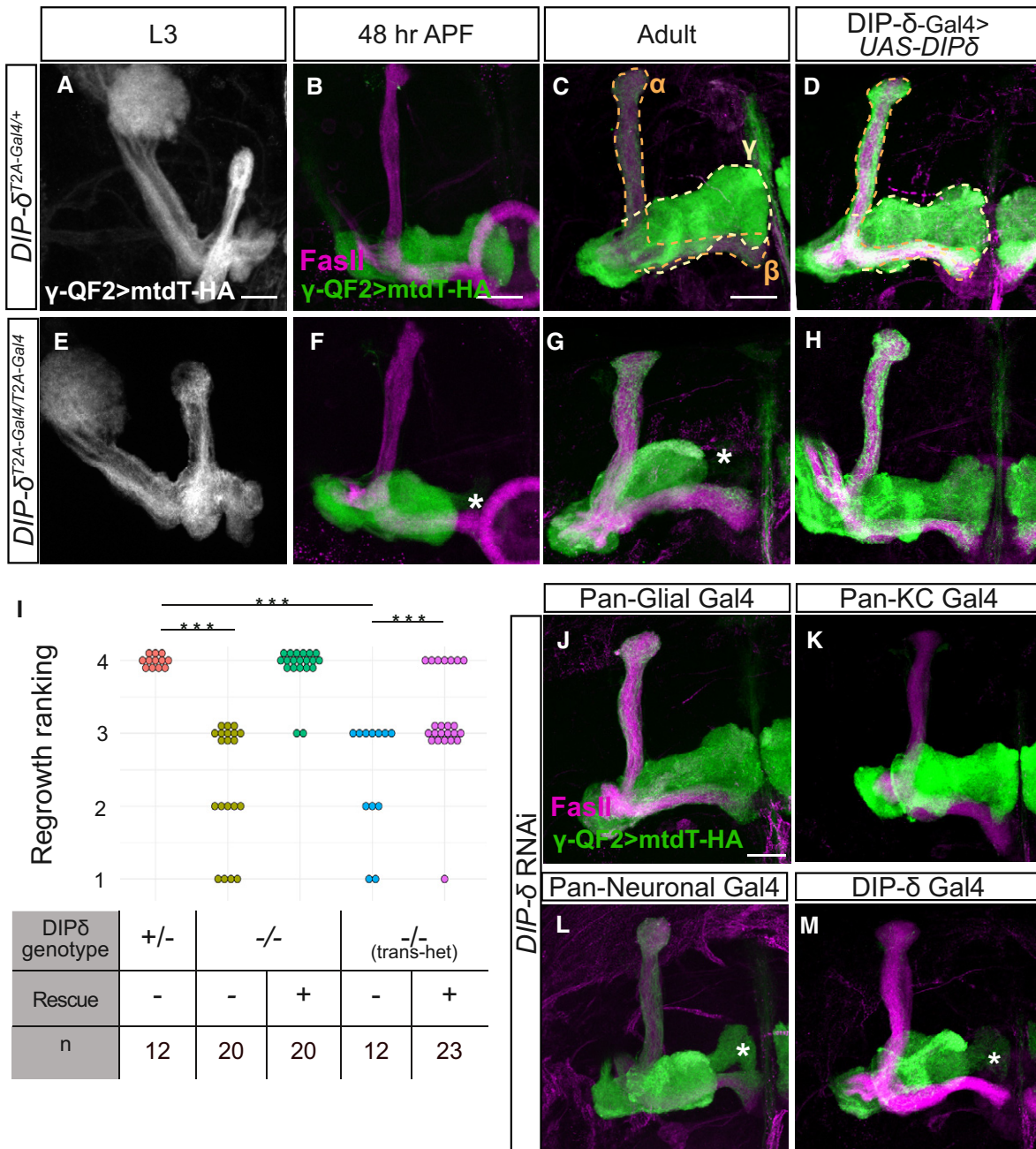


Figure 4. DIP-δ is required for γ-axon regrowth into the γ4/5 zones.

A–H Confocal z-projections *DIP-δ* hetero- and homozygous brains in which γ-KCs were labeled by expressing membrane-bound tandem tomato (mtdT-HA) driven by the γ-specific QF2 driver R71G10-QF2 (γ-QF2). Larval (L3) γ-axons grow normally in *DIP-δ^{T2A-Gal4}* heterozygotes (A; n = 16/16) and homozygotes (E; n = 24/24). In contrast, at 48 hr APF and adult, γ-axons within *DIP-δ^{T2A-Gal4}* homozygotes do not enter the distal part of the lobe (asterisks; F; n = 8/8, G; n = 20/20), while they grow normally in heterozygotes (B; n = 12/12, C; n = 12/12). Overexpression of a *DIP-δ* transgene driven by the Gal4 activity of *DIP-δ^{T2A-Gal4}* (see also Fig EV3) does not affect normal growth (D; n = 10/10) and rescues mutant phenotypes (H; n = 20/20). Note that while the R71G10 driver is consistently expressed in γ-KCs, it is also expressed in α/β-KCs in a stochastic manner. The adult γ-lobe and α/β lobes are outlined in (C, D) in yellow and orange, respectively, for clarity.

I Ranking of regrowth for (C, G, H), and Fig EV3D and E. Regrowth defect severity and statistics were calculated as in Fig 1; Wilcoxon–Mann–Whitney test; ***P < 0.001.

J–M Confocal z-projections of brains expressing *DIP-δ*-RNAi driven by the indicated Gal4. γ-KCs are labeled by mtdT-HA driven by R71G10-QF2 (γ-QF2). Expression of *DIP-δ*-RNAi in all glia (Repo-Gal4, J; n = 28/28) or all KCs (OK107-Gal4, K; n = 12/12) did not affect γ-neuron regrowth. In contrast, expression of *DIP-δ*-RNAi in all postmitotic neurons (C155-Gal4, L; n = 9/12) or *DIP-δ*-expressing neurons (*DIP-δ^{T2A-Gal4}*, M; n = 21/22) induced a defect in γ4/5 innervation by γ-axons.

Data information: Asterisks demarcate distal part of the lobe. Green and white are mtdT-HA, and magenta is FasII. Scale bar is 20 μm.

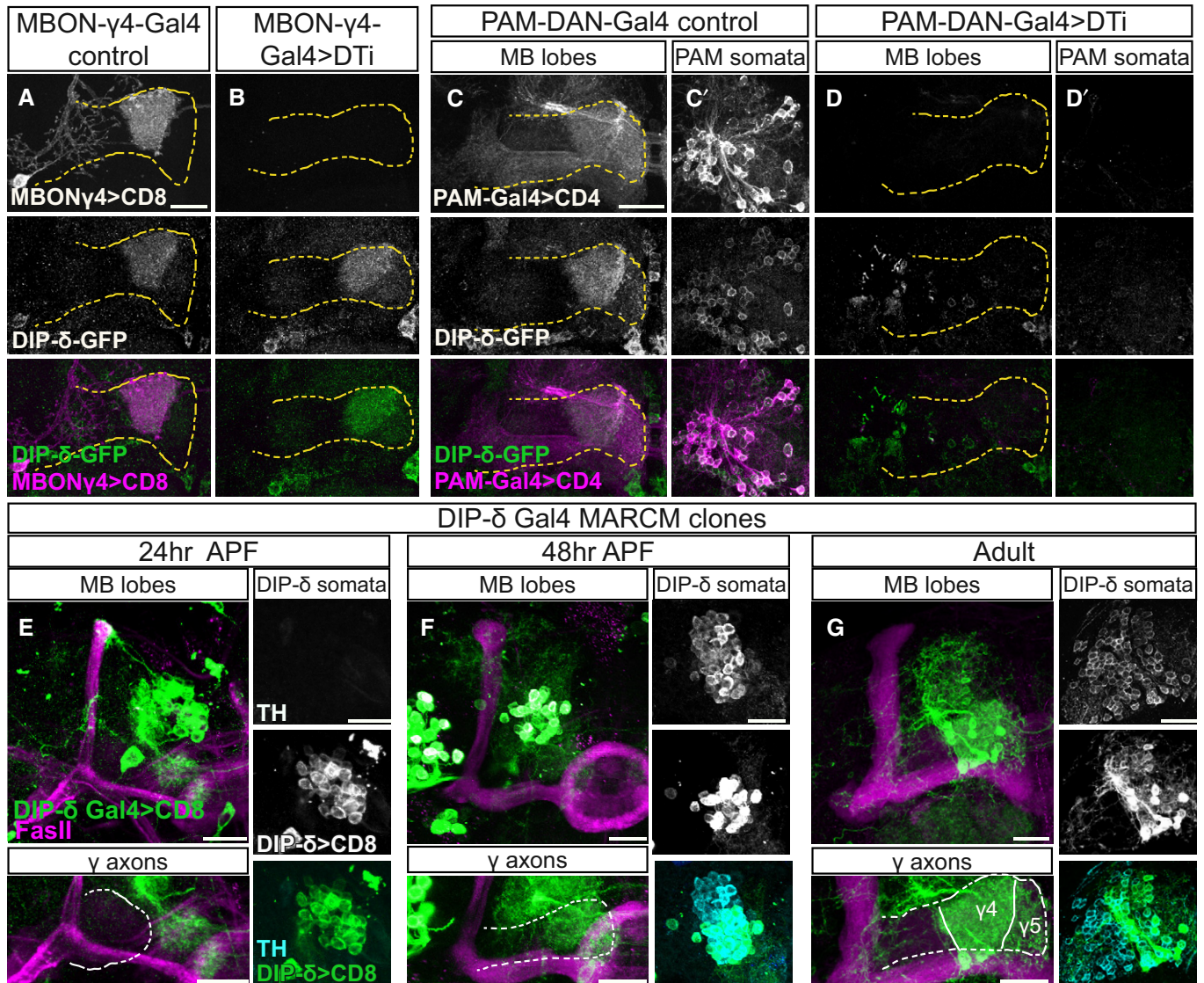


Figure 5. PAM-DANs are the source of DIP- δ in the γ 4/5 zones.

A–D Confocal z-projections of brains expressing DIP- δ ^{GFP} (DIP- δ -GFP) together with the indicated Gal4s and transgenes. Expressing diphtheria toxin (DTi) and membrane-bound RFP (mCD8-RFP; CD8) driven by the γ 4 > γ 1 γ 2 MBON driver MB294B-Gal4 (MBON γ 4-Gal4) did not affect DIP- δ -GFP expression (A, $n = 16/16$; B, $n = 14/14$). In contrast, similar expression of DTi and membrane-bound tomato (CD4-tdT; CD4) in PAM-DANs (using the GMR58E02-Gal4; PAM-DAN-Gal4) abolished the normal DIP- δ -GFP expression in the γ 4/5 zone (compare D, $n = 18/18$, to C, $n = 16/16$) and within the PAM-DAN cell bodies (compare D' to C'). Magenta is CD8-RFP (A, B) and CD4-tdT (C, D). Green is GFP, and grayscale depicts individual channels as labeled. Scale bar is 20 μ m. Yellow dashed line demarcates the γ -lobe based on FasII staining (not shown).

E–G Confocal z-projections of MARCM clones labeled by DIP- δ ^{T2A-Gal4} (DIP- δ Gal4) driving the expression of membrane-bound GFP (mCD8-GFP; CD8) and heat shocked at 24 h after egg laying. Clones innervate the γ 4/5 zones at 24 h APF (E; $n = 8$), 48 h APF (F; $n = 8$), and adult (G; $n = 16$). Clones become tyrosine hydroxylase (TH) positive only at 48 h APF onwards (F, G). Magenta is FasII, green is mCD8-GFP, cyan is TH antibody staining, and grayscale single channels are shown as indicated. White dashed line demarcates the γ -lobe. Scale bar is 20 μ m.

either *dpr12* or DIP- δ affects their binding partner localization and mature circuit architecture. First, we investigated whether the highly localized expression of Dpr12 and DIP- δ is cell-autonomous or requires interaction with their binding partner. We visualized Dpr12- and DIP- δ -GFP fusion proteins in brains homozygous mutant for their reciprocal Dpr/DIP partner. We found that Dpr12 expression appears diffuse in DIP- δ mutant brains throughout development

(Fig 6A–D, Appendix Fig S1C), indicating that Dpr12 protein localization requires interaction with DIP- δ , likely on PAM-DANs. In contrast, DIP- δ localization seemed unperturbed during the early stages of development in *dpr12* mutants (Fig 6E and F). At both 48 h and 72 h APF, while we still detected DIP- δ at the distal part of the lobe, it occupied a smaller area than in WT brains and resembled the innervation pattern typical of 24 h APF (compare Figs 6G

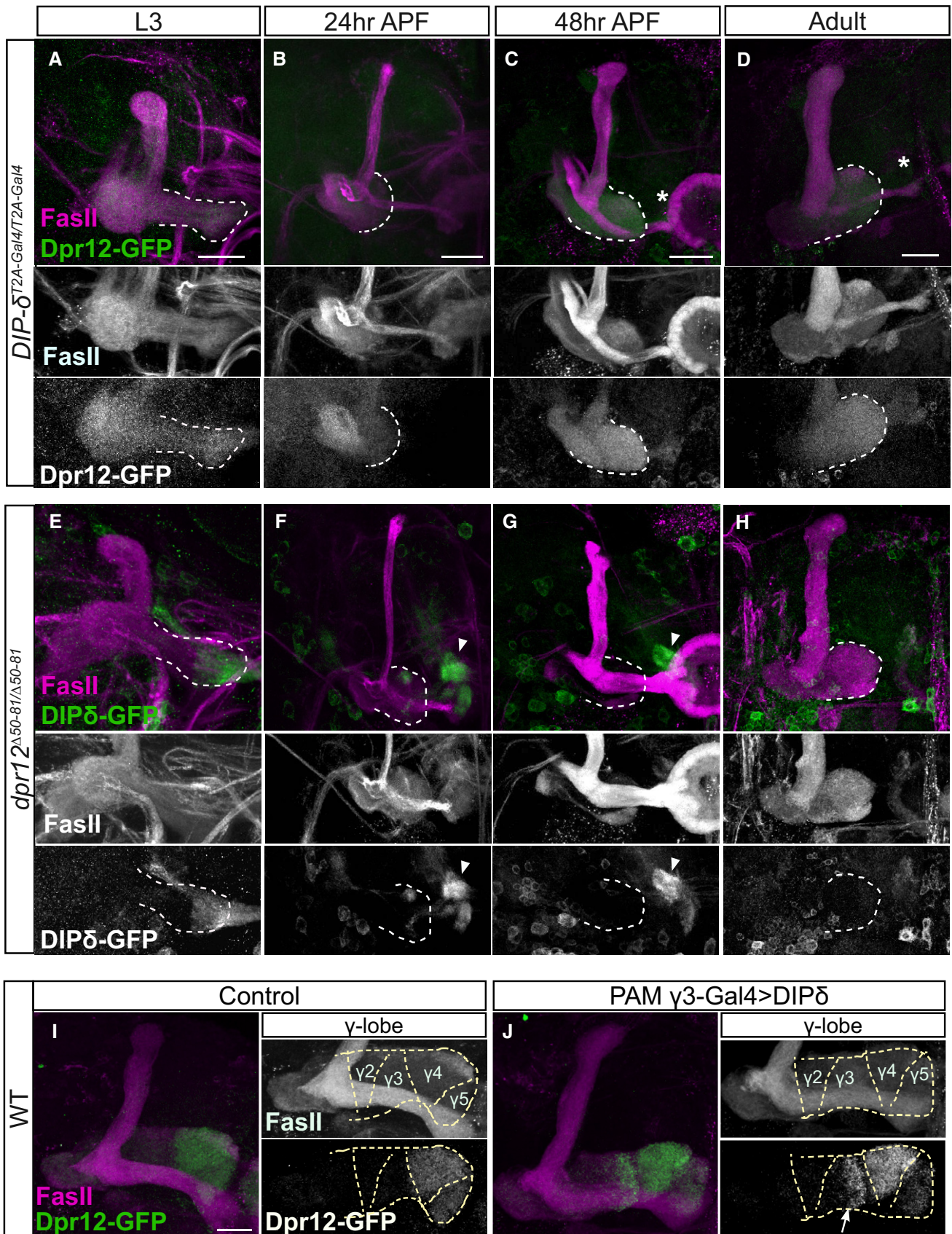


Figure 6.

Figure 6. DIP- δ is required and sufficient for Dpr12 localization.

A–J Confocal z-projections of brains expressing MiMIC mediated Dpr12^{G^{FTF}} (Dpr12-GFP) and DIP- δ ^{G^{FTF}} (DIP- δ -GFP) fusion proteins of the indicated genotypes and time points. (A–D) Dpr12-GFP expression is diffuse in *DIP- δ ^{T2A-Gal4}* homozygotes mutant brains at L3 (A; $n = 20/20$), 24 h APF (B; $n = 14/14$), 48 h APF (C; $n = 28/28$), and adult (D; $n = 26/26$). (E–H) DIP- δ -GFP expression in *dpr12 ^{Δ 50-81}* homozygotes mutant brains remains localized to the distal part of the γ -lobe at L3 (E; $n = 16/16$), 24 h APF (F; $n = 16/16$), and 48 h APF (G; $n = 10/10$) but cannot be identified in adult brains (H; $n = 16/16$). (I, J) Dpr12-GFP expression in WT animals (I, $n = 8/8$) or in those ectopically expressing DIP- δ in PAM-DANs that innervate the γ 3 zone (J, $n = 14/14$) driven by MB441B-Gal4 (PAM-DAN- γ 3-Gal4). DIP- δ expression in PAM-DAN- γ 3 resulted in Dpr12-GFP localization within the γ 3 zone (arrow), in addition to its normal γ 4/ γ 5 localization.

Data information: Arrowheads demarcate DIP- δ expression at the distal part of the lobe. Asterisks demarcate the distal part of the lobe. Dashed line depicts the medial γ -lobe, as determined by FasII staining. See legend of Fig EV1D for an explanation regarding the β -lobe morphological defects observed in (E, J). Green is GFP, and magenta is FasII. Grayscale panels represent single channels, as indicated. Scale bar is 20 μ m.

to 3G and Appendix Fig S1D to S1B). Furthermore, we did not detect any DIP- δ in the adult MB medial lobe (Fig 6H), suggesting that Dpr12 is required for the refinement and maintenance of DIP- δ localization.

To explore whether DIP- δ expression is sufficient to regulate Dpr12 protein localization within the γ -lobe, we misexpressed DIP- δ in PAM-DANs that innervate the γ 3 zone, normally devoid of Dpr12 protein (Fig 6I). Remarkably, we found that DIP- δ misexpression indeed caused Dpr12 protein to become localized to the adult γ 3 zone, in addition to its endogenous γ 4/ γ 5 localization (Fig 6J). Together, these results indicate that while DIP- δ is both required and sufficient for Dpr12 localization throughout development, Dpr12 is required only for maintenance of the adult localization of DIP- δ .

Dpr12-DIP- δ interaction mediates circuit re-assembly

We next determined whether the loss of normal Dpr12-DIP- δ interaction induced axonal misrouting, cell loss, or other circuit reorganizations. In *dpr12* mutants, we found that PAM-DANs which normally target the γ 4 or γ 5 zones misrouted and failed to form substantial connections within the γ -lobe (Figs 7A–D, and EV5A–E). Importantly, the number of PAM-DAN cell bodies of the subtypes tested remained unaffected in *dpr12* mutants, suggesting that the observed change is not associated with cell death (Fig EV5C and F). In contrast, the γ 4 > γ 1 γ 2-MBON still innervated the γ -lobe in *dpr12* mutant brains, albeit in abnormal locations like the γ 3 compartment (Figs 7E and F, and EV5G–I). As expected, the innervation pattern of an MBON targeting the γ 3 zone (MBON γ 3 β '1 or MBON-09) was unaffected by the *dpr12* mutant phenotype (Appendix Fig S2). Finally, we examined the global neuropil structure in *dpr12* mutant brains by following staining of the active zone protein bruchpilot (Brp), which demonstrated that the γ 4/ γ 5 zones were largely missing (Fig 7G and H, Movies EV4–EV5). Interestingly, the lack of these zones was accompanied by enlarged γ 2/ γ 3 zones, as well as distortions in other, adjacent brain regions. This was demonstrated, for example, with Crepine (Cre), a neuropil that surrounds the medial MB lobes and functions as a convergence zone for DAN dendrites and MBON axons (Aso et al, 2014a; Fig 7G and H). Whether the change in Crepine anatomy is a result of a direct function of Dpr12-DIP- δ specifically within the Crepine, or a secondary effect due to the lack of the γ 4–5 zones, remains to be determined.

Taken together, our data suggest that the Dpr12-DIP- δ interaction is required for circuit re-assembly between γ -KCs and PAM-DANs and is not required for PAM-DAN viability.

 γ 4/ γ 5 zone formation depends on matching Dpr-DIP-pairing between γ -KCs and PAM-DANs

To gain mechanistic insights into the Dpr12-DIP- δ interaction, we wanted to determine whether it is specifically required for the formation of the γ 4/ γ 5 zones, or, alternatively, could other similar interactions between γ -KCs and PAM-DANs mediate this process. First, we tested whether loss of the Dpr12-DIP- δ interaction could be compensated by other matching Dpr-DIPs. We focused on the interaction between Dpr6/Dpr10 and their interacting partner DIP- α (Carrillo et al, 2015), since both Dpr6 and Dpr10 are endogenously expressed in γ -KCs (Fig 1B; Alyagor et al, 2018), and DIP- α is largely absent from PAM-DANs (Croset et al, 2018; Aso et al, 2019). In a replacement experiment, we overexpressed DIP- α within DIP- δ -expressing neurons (using DIP- δ -Gal4), on a *DIP- δ ^{-/-}* background. Remarkably, this resulted in complete suppression of the *DIP- δ* mutant phenotype, and γ -axons now extended to the edge of the lobe (Fig 8A, B, and G, see additional controls in Fig EV6A and B). Thus, expression of DIP- α instead of DIP- δ is sufficient to rescue γ 4/5 innervation. While DIP- α likely interacts with Dpr6/Dpr10 in γ -KCs, in theory DIP- α could also function via Dpr12. To further explore this possibility, we performed two parallel experiments. First, we determined Dpr12 protein localization in this abnormal situation where DIP- δ is missing but γ -lobe morphology is seemingly normal. Indeed, we found that in this genetic background, Dpr12-GFP is no longer enriched in the γ 4/ γ 5 zones but instead diffused along the γ -lobe, suggesting DIP- α functions in a Dpr12-independent manner (Fig 8C and D). Second, we wanted to determine whether expression of DIP- α in addition to DIP- δ can suppress the *dpr12* mutant phenotype. Indeed, we found that overexpressing DIP- α within DIP- δ -expressing neurons, this time on a *dpr12^{-/-}* background, also led to suppression of the wiring defect, as well as restored the normal innervation pattern of PAM-DANs (see cyan in Fig 8E and F). Together, these findings suggest that formation of the γ 4/ γ 5 zones can be driven by matching Dpr-DIP-mediated interactions between γ -KCs and PAM-DANs, regardless of their specific identity.

Finally, since Dpr/DIPs are IgSF proteins, hence their interactions are expected to be, at least in principle, of adhesive nature, we examined whether another adhesive interaction between γ -KCs and PAM-DANs could replace the Dpr12-DIP- δ interaction. We focused on FasII, an IgSF adhesion molecule that forms homophilic interactions and is endogenously expressed in γ -KCs (Kurusu et al, 2002; Bornstein et al, 2015). However, overexpressing FasII within DIP- δ -expressing cells was not sufficient to suppress the *DIP- δ ^{-/-}* phenotype, and the γ 4/ γ 5 zones failed to form (Fig EV6C and D), indicating the specific requirement of Dpr-DIP-mediated interactions.

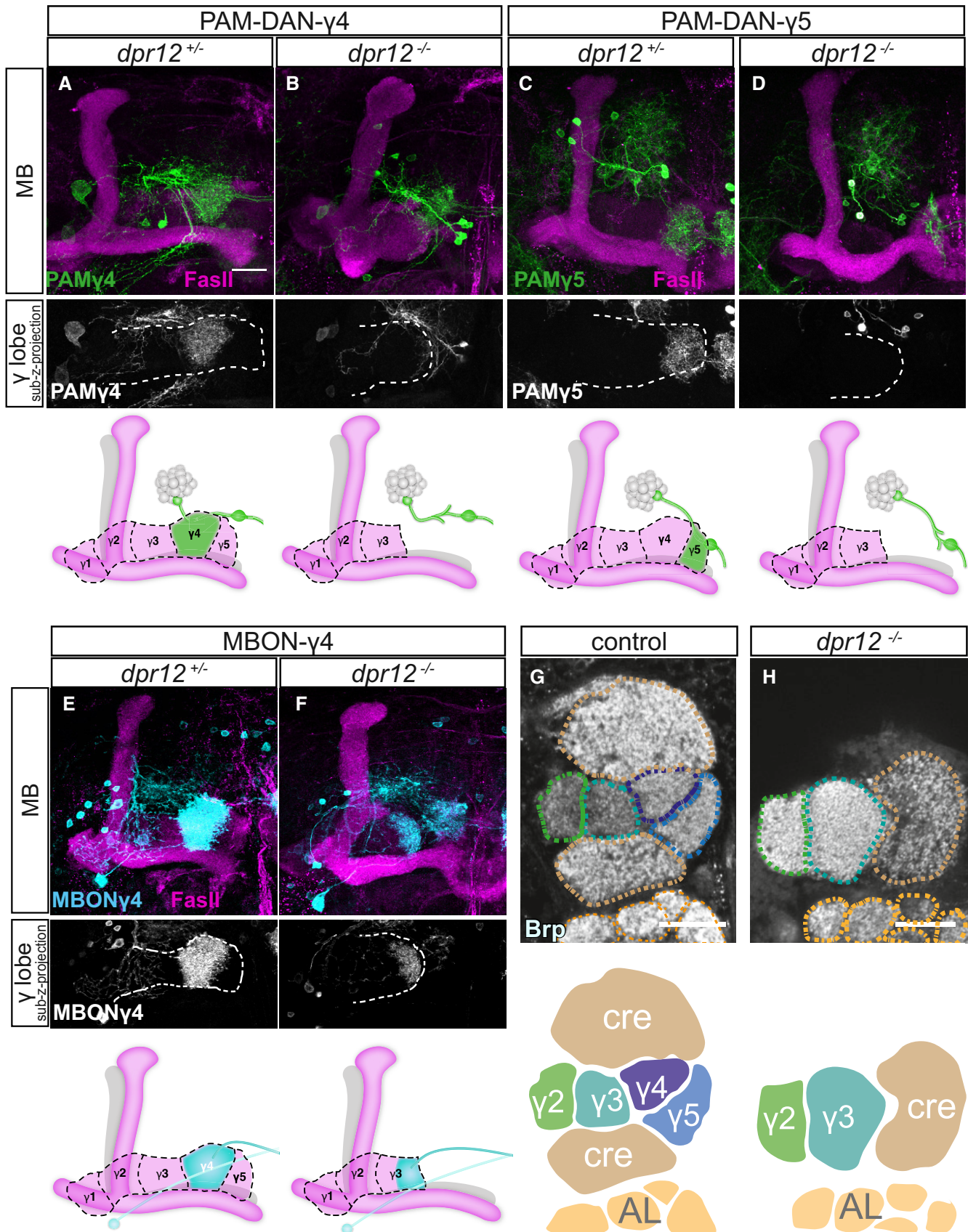


Figure 7.

Figure 7. Dpr12-DIP- δ interaction mediates circuit assembly.

A–F Top: Confocal z-projections of *dpr12* ^{Δ 50-81} heterozygous (A, $n = 15$; C, $n = 10$; E, $n = 10$) and homozygous brains (B, $n = 8$; D, $n = 18$; F, $n = 24$) expressing mCD8-GFP (CD8) driven by: (A, B) R10G03-Gal4 (PAM-DAN- γ 4-Gal4); (C, D) R48H11-Gal4 (PAM-DAN- γ 5-Gal4), or (E, F) R18H09-Gal4 (MBON γ 4 > γ 1 γ 2 -Gal4). The grayscale channels are sub-z-projections comprised of slices restricted to the γ -lobe region. White dashed line demarcates the γ -lobe. Bottom: Cartoons schematizing MB lobe structure and innervation by specific PAM-DANs or MBON.

G, H Single confocal slices of WT (G, $n = 5/5$) and *dpr12* ^{Δ 50-81} homozygous brains (H, $n = 5/5$) stained with anti-Brp. Dashed lines demarcate neuropil boundaries, schematic shown below. Cre, crepine, a neuropil that surrounds the medial MB lobes; AL, antenna lobe.

Data information: Magenta is FaslI, green and cyan are mCD8-GFP, and grayscale depicts single channels as indicated. Scale bar is 20 μ m.

Taken together, our data suggest that matching interactions between Dprs, expressed in γ -KCs, and DIPs, expressed in PAM-DANs, mediate the formation of the MB γ 4/5 zones, via a mechanism that is not solely based on adhesion.

Discussion

Our understanding of the development of complex neural circuits remains largely unknown. Specifically, how long axons can make *en passant* synapses with different partners in a stereotypic manner is not well understood. The unique development and morphology of the *Drosophila* MB γ -lobe, combined with the comprehensive genetic power of the fly, offer an excellent opportunity to dissect mechanisms required for wiring of complex neural networks, and specifically mechanisms that drive zonation within axonal bundles to allow for stereotypic localized innervation by distinct populations of neurons. Here, we identify a molecular mechanism that mediates neuron–neuron interactions which subsequently promote the formation of stereotypic circuits that define subcellular axonal zones.

The adult γ -lobe is divided into zones (also known as compartments) due to specific and localized innervations by extrinsic MB neurons including MBONs and DANs. Here we show that the interaction between two IgSF proteins, Dpr12 on γ -KCs and DIP- δ on PAM-DANs, underlies the formation of the MB γ 4/5 zones. Within each zone, input from DANs can modify synaptic strength between the KC and MBON to provide specific valence to sensory information (Aso *et al*, 2014a,b; Cohn *et al*, 2015; Cognigni *et al*, 2018). Based on the results presented here, we speculate that various specific combinations of adhesion molecules may mediate target recognition events that occur between predefined synaptic pairs in other MB zones as well. γ -neurons express a broad spectrum of IgSFs in tight temporal regulation (Dataset EV1; Alyagor *et al*, 2018), highlighting their potential role in circuit formation. However, many adhesion molecules, including Dpr/DIPs, can form promiscuous interactions, making their analyses challenging. Future studies could use CRISPR/Cas9 technology to generate multi-gene mutations to further explore the adhesion code required for zone/compartment formation.

Here we used the interaction between Dpr12 and DIP- δ to study the development of the γ 4/5 zones. Our developmental analyses have concluded that DIP- δ -expressing PAM-DANs arrive to the region of the γ 4/5 zones before γ -axons. Interestingly, our DIP- δ localization experiments suggest that in *dpr12* mutant animals, PAM-DANs arrive to the right place (the future γ 4/5 zones) during larval development, maintain their processes at least until 48 h APF, but eventually (at a yet unknown time point) eliminate or remodel their γ 4/5 innervations, while maintaining and even strengthening/

broadening other connections in this vicinity. Therefore, it is attractive to speculate that γ -axons extend into a prepatterned lobe. More studies comparing the development of other compartment-specific DANs as well as MBONs are however required.

Here we demonstrate that Dpr12 is cell-autonomously required in γ -KCs, while DIP- δ is required in PAM-DANs for the formation of the γ 4/5 zones. To the best of our knowledge, this is the first case in which a Dpr molecule was shown to be cell-autonomously required for correct wiring. However, the precise molecular mechanism by which the Dpr12-DIP- δ interaction mediates formation of the γ 4/5 zones, or, in fact, how any wiring by Dpr-DIPs is achieved, is yet to be determined. The robust phenotype associated with loss of the Dpr12-DIP- δ interaction offers an excellent opportunity to delve into the mechanistic basis, which could potentially shed light on similar mechanisms in the visual system and the NMJ. Further research should focus on several critical questions that remain unresolved: (i) Why do the γ -axons stop prematurely? That γ -axons stall at the γ 3- γ 4 junction when we perturb the Dpr12-DIP- δ interaction—which at least in principle is expected to be of adhesive nature—is unintuitive. One possibility is that axon growth into the γ 4/5 zones depends on Dpr12-DIP- δ interaction either because they overcome a yet undiscovered inhibitory signal, or because they are positively required for the progression of the growth cone. Alternatively, Dpr12-DIP- δ interaction could be important for the stabilization of the connections between γ -axons and PAM-DAN processes to result in the formation of the γ 4/5 zones. At 48 h APF, the large majority of *dpr12* mutant γ -axons do not innervate the γ 4/5 zones, arguing against the stability hypothesis; (ii) What are the signaling pathways that mediate Dpr/DIP targeting recognition? None of the Dprs or DIPs contain a large intracellular domain that is capable of signaling. Identifying the potential co-receptor/s is a critical step in gaining a mechanistic understanding of axon targeting whether in the visual, motor or MB circuits. Our results that DIP- α can replace DIP- δ suggest that signaling may be conserved between different Dpr-DIP pairs; (iii) What is the significance of the GPI anchor? Many of the Dprs and DIPs are predicted to be GPI-anchored proteins (e.g., Cheng *et al*, 2019), suggesting that they can be cleaved to create a secreted soluble form. Whether this is an important step in targeting has not yet been investigated. Interestingly, the vertebrate homologs of the DIPs, the IgLON subfamily (Zinn & Ozkan, 2017), are GPI-anchored proteins that were shown to be cut by metalloproteinases to promote axonal outgrowth (Sanz *et al*, 2015).

Expression patterns of Dpr and DIP molecules in the NMJ (Carrillo *et al*, 2015) and visual system (Carrillo *et al*, 2015; Tan *et al*, 2015) suggested a model where these molecules instruct target cell specificity. Recent loss-of-function experiments strengthened this

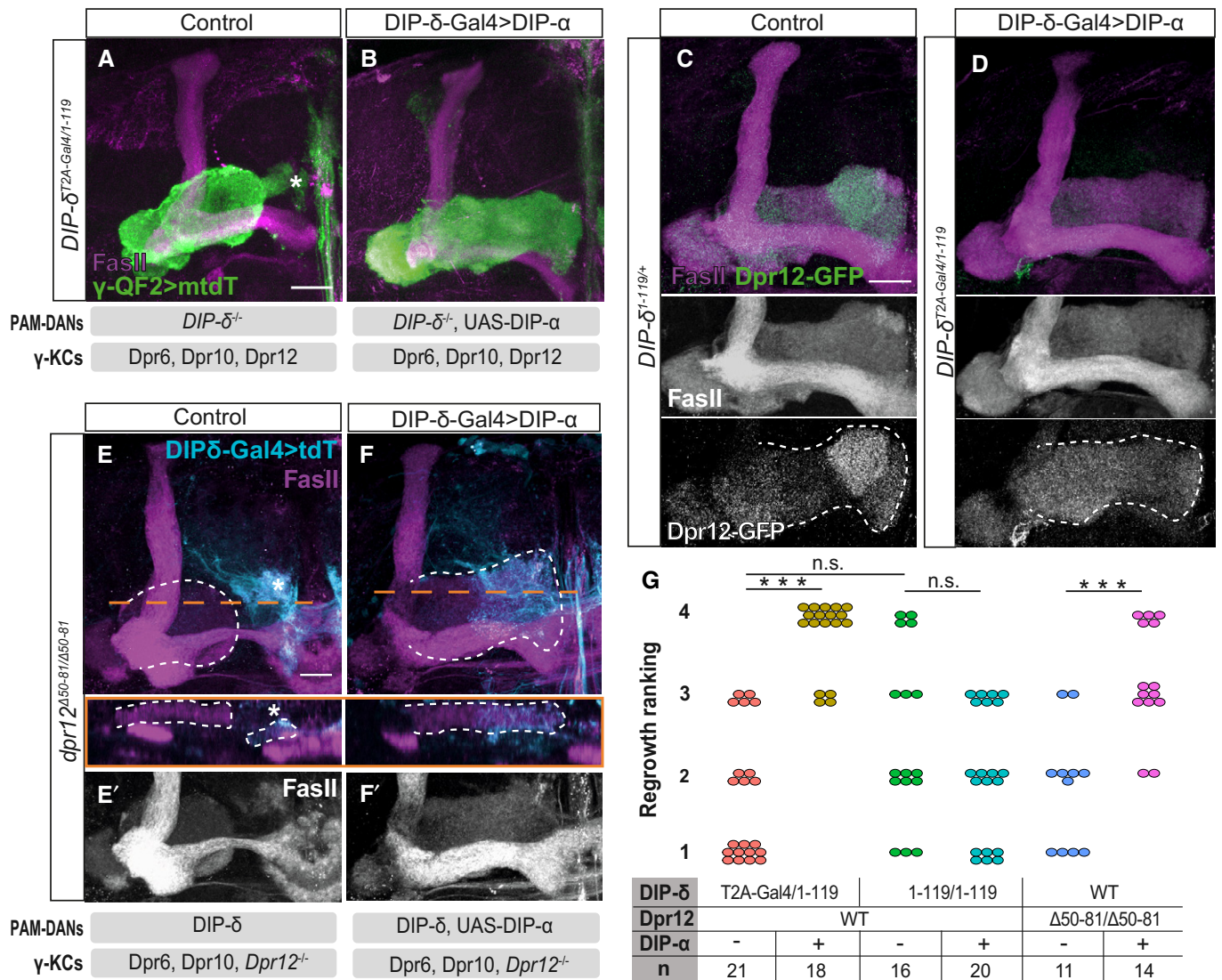


Figure 8. γ 4/5 zone formation depends on matching Dpr-DIP-pairing between γ -KCs and PAM-DANs.

A, B Confocal z-projections of adult *DIP- δ ^{T2A-Gal4/1-119}* trans-heterozygous mutant brains, in which γ -KCs are labeled by membrane-bound tandem tomato (mtdT-HA; green) driven by R71G10-QF2 (γ -QF2), and DIP- δ -Gal4 (expressed in DIP- δ ⁺ neurons) either drives expression of UAS-DIP- α (B) or not (A). Gray boxes below the images describe the relevant components within PAM-DANs and γ -KCs.

C, D Confocal z-projections of adult *DIP- δ ^{T2A-Gal4/1-119}* trans-heterozygous mutant (D) or *DIP- δ ^{1-119/1-119}* heterozygous (C) brains, which express MiMIC mediated Dpr12^{CFSTF} (Dpr12-GFP; green). In (D), DIP- δ -Gal4 drives expression of UAS-DIP- α . Grayscale panels represent single channels, as indicated. The γ -lobe is outlined in white.

E, F Confocal z-projections of adult *dpr12^{Δ50-81}* homozygous mutant brains, in which DIP- δ -Gal4 drives expression of either UAS-*mtdT* (E) or UAS-DIP- α -T2A-*tdT* (F; expected to induce expression of DIP- α as well as tdT encoded by a polycistronic message). In orange are longitudinal sections across the γ -lobe at the indicated location. The γ -lobe is outlined in white, as determined by FasII staining (gray in E'-F'). Cyan is tdT within DIP- δ ⁺ cells. Gray boxes below the images describe the relevant components within PAM-DANs and γ -KCs.

G Ranking of regrowth for (A, B, E, F) and Fig EV6A and B. Regrowth defect severity and statistics were calculated as in Fig 1; Wilcoxon–Mann–Whitney test; ****P* < 0.001; ns, not significant.

Data information: In all images, magenta is FasII. Asterisks demarcate the distal part of the lobe. Scale bar is 20 μ m.

target specificity hypothesis, as the DIP- α -Dpr10 interaction was shown to be important for motoneuron innervation of specific larval (Ashley *et al*, 2019) and adult (Venkatasubramanian *et al*, 2019) muscles, and DIP- α -Dpr10/Dpr6 interactions for specific layer targeting in the visual system (Xu *et al*, 2018). Our results suggest that mechanisms used to target axons and dendrites to specific cell types

or layers may be further implicated to orchestrate the wiring of long axons to different pre- and postsynaptic partners along their route and thus the formation of axonal zones.

Here we describe that interaction between two IgSF proteins mediates transneuronal communication that is required for proper wiring within specific zones of the *Drosophila* MB. The anatomical

organization of the MB suggests that these interactions may provide target specificity for the long KC axon, while it forms *en passant* synapses with different targets along its length. While the existence of such wiring architecture is known from invertebrates such as *Drosophila* and *C. elegans*, long axons making distinct yet stereotypic *en passant* connections are not widely described in vertebrates. Given the existence of long axons, that travel through dense neuropil structures, such as mossy fibers in the

hippocampus, cholinergic axons in the basal forebrain, and parallel fibers in the cerebellar cortex, we posit that this type of connectivity exists in vertebrates but has not yet been described in detail due to technological limitations that are likely to be resolved soon. Pairwise IgSF-mediated molecular interactions are conserved in vertebrates and invertebrates, implying similar mechanisms to dictate axon and dendrite targeting of subcellular neurite zones in other organisms.

Materials and Methods

Reagents and Tools Table

REAGENT or RESOURCE	SOURCE	IDENTIFIER
Antibodies		
Chicken anti GFP 1:500	AVES	GFP-1020 RRID: AB_10000240
Mouse monoclonal anti FasII 1:25	Developmental Studies Hybridoma Bank (DSHB)	1D4 RRID: AB_528235
Mouse monoclonal anti Brp 1:5	DSHB	nc82 RRID: AB_2314866
Rabbit anti TH 1:500	Merck Millipore	AB152 RRID: AB_390204
Rat anti RFP 1:500	ChromoTek	5f8 RRID: AB_2336064
Alexa fluor 568 Goat anti Rat 1:500	Invitrogen	A-21247 RRID: AB_2534121
Alexa fluor 647 Goat anti Mouse 1:500	Invitrogen	A-32728 RRID: AB_2633277
Alexa fluor 488 Goat anti Mouse 1:500	Invitrogen	A-11001 RRID: AB_2534069
FITC Goat anti Chicken 1:500	Invitrogen	A-16055 RRID: AB_2534728
Alexa fluor 568 Goat anti Rabbit 1:500	Invitrogen	A-11036 RRID: AB_10563566
Bacterial and Virus Strains		
DH5 α		
Chemicals, Peptides, and Recombinant Proteins		
Cell Dissociation Solution	Sigma Aldrich	Cat# C1544
Collagenase/Dispase mix	Roche	Cat# 10269638001
poly-L-lysine	Sigma Aldrich	Cat# P1524-25MG
Critical Commercial Assays		
Pico pure RNA isolation kit	Thermo Fisher	Cat# KIT0204
Gibson assembly	NEB	Cat# E5510S
Deposited Data		
Raw data files for UNF Perturbation seq	Deposited in the NCBI Gene Expression Omnibus (https://www.ncbi.nlm.nih.gov/geo/query/acc.cgi?acc=GSE165896)	
Experimental Models: <i>D. melanogaster</i>		
<i>w</i> [1118]; <i>P</i> [y[+ <i>t7.7</i>] <i>w</i> [+ <i>mC</i>]= <i>GMR71G10-GAL4</i>]attP2 (<i>R71G10-Gal4</i>)	Bloomington <i>Drosophila</i> Stock Center (BDSC)	BDSC: 39604 FlyBase ID (FBID): FBsf0000166728

Reagents and Tools table (continued)

REAGENT or RESOURCE	SOURCE	IDENTIFIER
y^*, w^* ; $P\{y[+t7.7] w[+mC]=GMR71G10-GAL4\}attP40$	(Alyagor et al, 2018)	N/A
$P\{GawB\}elav^{C155}$ (C155-GAL4)	BDSC	BDSC: 458 FBID: FBti0002575
w^{1118} ; $P\{GAL4\}repo/TM3, Sb1$ (Repo-Gal4)	BDSC	BDSC: 7415 FBID: FBti0018692
$w[1118]$; $P\{y[+t7.7] w[+mC]=GMR58E02-GAL4\}attP2$ (R58E02-Gal4)	BDSC	BDSC: 41347 FBID: FBtp0061564
$w[1118]$; $P\{y[+t7.7] w[+mC]=GMR18H09-GAL4\}attP2$ (R18H09-Gal4)	BDSC	BDSC: 48830 FBID: FBti0133650
$w[1118]$; $P\{y[+t7.7] w[+mC]=GMR48H11-GAL4\}attP2$ (R48H11-GAL4)	BDSC	BDSC: 50396 FBID: FBti0136291
$w[1118]$; $P\{y[+t7.7] w[+mC]=GMR10G03-GAL4\}attP2$ (R10G03-Gal4)	BDSC	BDSC: 48271 FBID: FBti0132904
$P\{y[+t7.7] w[+mC]=GMR71G10-QF2^{HSP}\}attP40$ (R71G10-QF2)	This study	N/A
$y[1] w[*]$; $PBac\{y[+mDint2] w[+mC]=10XQUAS-6XGFP\}VK00018$, $P\{w[+mC]=UAS-mtdTomato-3xHA\}2$; $P\{y[+t7.7] w[+mC]=GMR58E02-QF2.L\}attP2$ (R58E02-QF2)	BDSC	BDSC: 66480 FBID: FBti0184753
$w[1118]$; $P\{y[+t7.7] w[+mC]=R53C03-p65.AD\}attP40$; $P\{y[+t7.7] w[+mC]=R24E12-GAL4.DBD\}attP2/TM6B, Tb[1]$ (MB298B-Gal4)	BDSC	BDSC: 68309 FBID: FBst0068309
$w[1118]$; $P\{y[+t7.7] w[+mC]=R30G08-p65.AD\}attP40$; $P\{y[+t7.7] w[+mC]=R48B03-GAL4.DBD\}attP2$ (MB441B-Gal4)	BDSC	BDSC: 68251 FBID: FBst0068251
$w[*]$; $P\{w[+mW.hs]=GawB\}OK107 ey[OK107]$ (OK107-Gal4)	BDSC	BDSC: 854 FBID: FBti0004170
$w[1118]$; $P\{y[+t7.7] w[+mC]=R94B10-GAL4.DBD\}attP2 PBac\{y[+mDint2] w[+mC]=R52G04-p65.AD\}VK00027$ (MBO83C-Gal4)	BDSC	BDSC: 68287 FBID: FBst0068287
y^*, w^* ; $DIP-\delta-T2A-Gal4$	This study	N/A
$w[*]$; $P\{y[+t7.7] w[+mC]=10XUAS-IVS-mCD8::GFP\}attP2$ (UAS-CD8-GFP)	BDSC	BDSC: 32185 FBID: FBst0032185
$w[*]$; $P\{y[+t7.7] w[+mC]=10XUAS-IVS-mCD8::GFP\} attP40$ (UAS-CD8-GFP)	BDSC	BDSC: 32186 FBID: FBst0032185
$y[1] w[*]$; $P\{y[+t7.7] w[+mC]=10XUAS-IVS-mCD8::GFP\}su(Hw)attP8$ (UAS-CD8-GFP)	BDSC	BDSC: 32189 FBID: FBst0032189:
$y[1] w[*]$; $P\{w[+mC]=UAS-CD4-tdTom\}7M1$ (UAS-CD4-tdT)	BDSC	BDSC: 35841 FBID: FBst0035841
$y[1] w[1118]$; $P\{w[+mC]=QUAS-mtdTomato-3xHA\}26$ (QUAS-mtdT)	BDSC	BDSC: 30005 FBID: FBti0129951
$w[1118]$; $P\{w[+mC]=UAS-Dcr-2.D\}10$	BDSC	BDSC: 24651 FBID: FBst0024651
$P\{hsFLP\}22, w^*$, $P\{w[+mC]=UAS-mCD8::GFP.L\}$; $P\{w[+mC]=tubP-GAL80\}LL10 P\{ry[+t7.2]=neoFRT\}40A$; $GMR71G10-Gal4$, $P\{w[+mC]=UAS-Dcr-2.D\}10$ (recombination between R71G10-Gal4 and UAS-Dcr-2)	This study	N/A FBID: FBfr0227179
$P\{hsFLP\}22, w^*$, $P\{w[+mC]=UAS-mCD8::GFP.L\}$; $P\{w[+mC]=tubP-GAL80\}LL10 P\{ry[+t7.2]=neoFRT\}40A$; $DIP-\delta-T2A-Gal4$	This study	N/A
$y[1] v[1]$; $P\{y[+t7.7] v[+t1.8]=TRiP.JF03306\}attP2$ (RNAi of Dpr5)	BDSC	BDSC: 29627 FBID: FBst0029627
$y[1] v[1]$; $P\{y[+t7.7] v[+t1.8]=TRiP.JF03172\}attP2$ (RNAi of Dpr8)	BDSC	BDSC: 28744 FBID: FBst0028744
$y[1] sc[*] v[1]$; $P\{y[+t7.7] v[+t1.8]=TRiP.HMS00288\}attP2$ (RNAi of Dpr9)	BDSC	BDSC: 33409 FBID: FBst0033409
$y[1] v[1]$; $P\{y[+t7.7] v[+t1.8]=TRiP.JF02920\}attP2$ (RNAi of Dpr10)	BDSC	BDSC: 27991 FBID: FBst0027991

Reagents and Tools table (continued)

REAGENT or RESOURCE	SOURCE	IDENTIFIER
y[1] v[1]; P{y[+t7.7] v[+t1.8]=TRiP.JF03210}attP2 (RNAi of Dpr12)	BDSC	BDSC: 28782 FBID: FBst0028782
[1] v[1]; P{y[+t7.7] v[+t1.8]=TRiP.GL01238}attP2 (RNAi of Dpr17)	BDSC	BDSC: 41656 FBID: FBst0041656
y[1] v[1]; P{y[+t7.7] v[+t1.8]=TRiP.JF03283}attP2 (RNAi of Dpr18)	BDSC	BDSC: 29604 FBID: FBst0029604
[1] v[1]; P{y[+t7.7] v[+t1.8]=TRiP.JF02923}attP2 (RNAi of Dpr20)	BDSC	BDSC: 28293 FBID: FBst0028293
P{ry[+t7.2]=hsFLP}12, y[1] w[*]; P{y[+t7.7] w[+mC]=UAS-Cas9.P2}attP40	BDSC	BDSC: 58985 FBID: FBst0058985
w[1118]; P{y[+t7.7] w[+mC]=UAS-Cas9.C}attP2	BDSC	BDSC: 54595 FBID: FBst0054595
gRNA dpr12	This study	N/A
y[1] sc[*] v[1]; P{y[+t7.7] v[+t1.8]=TKO.GS02451}attP40 (gRNA DIP- δ)	BDSC	BDSC: 78754 FBID: FBst0078754
y*,w*;FRT40A, dpr12 ^{A50-81} , FRTG13, cn,bw	This study	N/A
w*; DIP δ ¹⁻¹¹⁹ , FRT2A	A generous gift from Larry Zipursky, UCLA	N/A
y[1] w[67c23]; Mi{PT-GFSTF.1}dpr12[MIO1695-GFSTF.1]/SM6a (dpr12 ^{GFSTF})	BDSC	BDSC: 60171 FBID: FBst0060171
y[1] w[*]; Mi{PT-GFSTF.1}DIP-delta[MIO8287-GFSTF.1] (DIP- δ ^{GFSTF})	BDSC	BDSC: 60558 FBID: FBst0060558
y[1] w[*]; Mi{y[+mDint2]=MIC}DIP-delta[MIO8287]	BDSC	BDSC: 51229 FBID: FBst0051229
y[1] w[*]; P{w[+mC]=lox(Trojan-GAL4)x3}10; Dr[1]/TM3, Sb[1] Ser[1]	BDSC	BDSC: 60310 FBID: FBst0060310
P{y[+mDint2]=Crey}1b, y[1] M{uas-int. Dm}ZH-2A w[*]	BDSC	BDSC: 60299 FBID: FBst0060299
w[*]; P{w[+mC]=UAS-Cbeta\DT-A.1}18/CyO (UAS-DTI)	BDSC	BDSC: 25039 FBID: FBst0025039
UAS-Dpr12 (in86FB)	This study	N/A
UAS-DIP- δ (in attp40)	This study	N/A
UAS-DIP- δ -T2A-tdT	A generous gift from Larry Zipursky, UCLA	N/A
UAS-DIP- α	A generous gift from Larry Zipursky, UCLA	N/A
UAS-DIP- α -T2A-tdT	A generous gift from Larry Zipursky, UCLA	N/A
UAS-FasII-A	A generous gift from Brian McCabe (Beck et al, 2012)	N/A
y[1] M{w[+mC]=nos-Cas9.P}ZH-2A w[*]	BDSC	BDSC: 54591 FBID: FBst0054591
UAS-DIP- δ -RNAi (in attp40)	This study	N/A
y[1] w[*] P{y[+t7.7] w[+mC]=10XUAS-IVS-mCD8::RFP}su(Hw)attP8	BDSC	BDSC: 32220 FBID: FBst0032220
Oligonucleotides		
gRNAs for Dpr12 CRISPR deletion: CGCAGTTCCATCAGGTGCAGGG CCATTAGACATATCTTCTGACC	This study	N/A
Primers for dpr12 ^{A50-81} check PCR: F':GTTGCCGTAGCTGAAAGGATT R':TAAACCGGTATCGGAGTGTC	This study	N/A

Reagents and Tools table (continued)

REAGENT or RESOURCE	SOURCE	IDENTIFIER
RNAi for DIP δ (SS) GACGAUAAGAAACCUACAUA (AS) UUGUAGGUUUUCUUAUCGUCAG	This study	N/A
Primers for QF2 cloning F: TAAGCCAACCTTTGAATCACAAGACGCATACCAACGGTACATGCCACCCAAG R: TGAATAATTTTCTATTTGGCTTTAGTCGACGGTATCGATAATCACTGTTCTG	This study	N/A
Primers for hsp70 cloning F':AAGTGGTGATAAACGGCCGCCGAGCGCCGAGTATAAATAGAG R':AAGTGGTGATAAACGGCCGCCGAGCGCCGAGTATAAATAGAG	This study	N/A
Recombinant DNA		
pCFD4	(Port <i>et al</i> , 2014)	N/A
pVALIUM22	Harvard Medical School	PlasmID: pVALIUM22
pDEST-UAS-IVS-Syn21-p10aw	(Rabinovich <i>et al</i> , 2016)	N/A
pBPGUw	addgene	Plasmid #17575
pBPGUw-QF2	This study	N/A
GMR71G10 entry vector	(Alyagor <i>et al</i> , 2018)	N/A
GMR71G10-QF2 ^{hsp70}	This study	N/A
Plasmid: UAS-IVS-Syn21-Dpr12-p10	This study	N/A
Plasmid: UAS-IVS-Syn21-DIP- δ -p10	This study	N/A
Plasmid: pCFD4-dpr12 (Dpr12 gRNA)	This study	N/A
Plasmid: pVALIUM22-DIP- δ (DIP- δ RNAi)	This study	N/A
Software and Algorithms		
Fiji	Image J	https://imagej.net/Fiji/Downloads
VVD Viewer (a branch of FluoRender, Center for Integrative Biomedical Computing (CIBC), Utah)	Takashi Kawase	https://github.com/takashi310/VVD_Viewer/releases
MATLAB R2016a software	MathWorks	N/A
FlyMine	(Lyne <i>et al</i> , 2007)	http://www.flymine.org/
HISAT v.0.1.5	(Kim <i>et al</i> , 2015)	https://github.com/infphilo/hisat
DESeq2	(Love <i>et al</i> , 2014)	N/A
Gene-e v.3.0.215	Broad Institute, Inc.	https://software.broadinstitute.org/GENE-E/
HOMER software	(Heinz <i>et al</i> , 2010)	
DSIR	(Vert <i>et al</i> , 2006)	http://biodev.extra.cea.fr/DSIR/DSIR.php
FlyCRISPR	(Gratz <i>et al</i> , 2014)	http://flycrispr.molbio.wisc.edu/
neuPrint	(Clements <i>et al</i> , 2020)	https://neuprint.janelia.org/
Other		
Zeiss LSM 800 confocal microscope	Zeiss	
40 \times 1.3 NA oil immersion lens	Zeiss	

Methods and Protocols

Experimental model

Drosophila melanogaster flies were reared under standard laboratory conditions at 25°C on molasses containing food. Males and females were chosen at random. For developmental analysis, white pupae were collected and incubated for the indicated number of hours. For adult analysis, flies were dissected 3–5 days posteclosion.

See Appendix: List of genotypes for the detailed list of all fly genotypes used in this study.

RNA extraction

The RNA extraction of WT and UNF-RNAi-expressing MB γ -KCs was performed as described in Alyagor *et al* (2018). In brief, brains were dissected in a cold Ringer's solution and dissociated by incubation with collagenase/dispase mix at 29°C (Roche, 15 min for larval and pupal brains and 30 min for adult brains), washed in dissociation solution (Sigma-Aldrich), and mechanically dissociated into single cells. Cells were transferred via 35 μ m mesh (Falcon) to eliminate clusters and debris. 1,000 γ -KCs (DsRed⁺) were sorted using a 100 mm nozzle and low pressure in BD FACSAria Fusion (BD

Bioscience) directly into 100 μ l Pico-Pure RNA isolation kit extraction buffer (Life Technologies) followed by RNA extraction. mRNA was captured using 12 ml of Dynabeads oligo (Life Technologies), which were washed from unbound total RNA according to the protocol. mRNA was eluted from beads at 85°C with 10 ml of 10 mM Tris-HCl (pH 7.5). mRNA was barcoded, converted into cDNA, and linearly amplified by T7 *in vitro* transcription. The resulting RNA was fragmented and converted into an Illumina sequencing-ready library through ligation, RT, and PCR. Prior to sequencing, libraries were evaluated by Qubit fluorometer and TapeStation (Agilent).

Analysis of RNA-seq Data

Samples were sequenced using Illumina NextSeq 500, at a sequencing depth of an average of 5 million reads. We aligned the reads to *D. melanogaster* reference genome (DM6, UCSC) using Hisat v0.1.5 with “-sensitive -local” parameters (Kim *et al*, 2015). Gene annotation was taken from FlyBase.org (Dmel R6.01/Fb_2014_04). Duplicate reads were filtered if they aligned to the same base and had identical unique molecular identifiers (UMI). Expression levels were counted using HOMER software (<http://homer.salk.edu>) (Heinz *et al*, 2010). For general analyses, we considered genes with reads over the noise threshold (20 reads). Significant expression in γ -KCs was considered for genes with reads over a second noise threshold (50 reads) in at least two γ -KCs. For normalization and statistics, we performed DEseq2 algorithm (Love *et al*, 2014) on our samples on R platform, which took into account batch effects. All *P*-values presented for RNA-seq data are adjusted *P*-values. Gene enrichment analysis was done using FlyMine (<http://www.flymine.org/>).

Generation of CRISPR-mediated mutant

For Dpr12 mutation, two guide RNAs were designed using the FlyCRISPR algorithm (<http://flycrispr.molbio.wisc.edu/>) and cloned into pCFD4 using Transfer-PCR (TPCR) (Unger *et al*, 2010; Meltzer *et al*, 2019). The pCFD4-Dpr12 plasmid was injected into the 86FB landing site using Φ C31 integration (BestGene). Injected flies were crossed with nanos-Cas9 flies (Bloomington stock #54591). After two generations, single males were crossed with balancers and checked for deletion using specific primers. The dpr12^{Δ50-81} allele is a 32bp deletion in the 5' end of the transcript resulting in a premature stop after 37aa.

For tissue-specific CRISPR (tsCRISPR), Dpr12- and DIP- δ gRNA-containing flies were crossed with UAS-Cas9.C or UAS-Cas9.P2, respectively, driven by the indicated Gal4s.

Generation of transgenes and transgenic flies

To generate UAS-Dpr12 and UAS-DIP- δ transgenes, cDNA was cloned into the Gateway entry vector pDONR201. The Gateway entry vectors were then recombined into pDEST-UAS-IVS-Syn21-p10aw destination vector (Rabinovich *et al*, 2016) using LR recombinase (Invitrogen). UAS-Dpr12 and UAS-DIP- δ plasmids were injected into the 86FB and attp40 landing sites, respectively, using Φ C31 integration (BestGene).

For the generation of UAS-DIP- δ RNAi, a 21 nucleotide sequence was selected using DSIR (<http://biodev.extra.cea.fr/DSIR/DSIR.php>). Off-target results were eliminated by blast in NCBI. The RNAi hairpins were cloned into pVALIUM22 as described in <https://fgr.hms.harvard.edu/cloning-and-sequencing>. In brief, hairpin oligos,

containing sense and anti-sense nucleotide with overhang DNA fragment for *NheI* and *EcoRI*, were synthesized (Sigma). 10 μ l of sense and anti-sense strand oligos (10–20 μ M each) were annealed into 80 μ l annealing buffer (10 mM Tris-HCl, pH 7.5, 0.1 M NaCl, 1 mM EDTA) by incubation at 95°C for 5 min. 6 μ l of the annealed oligos were directly cloned into the pVALIUM22 vector which has been linearized by *NheI* and *EcoRI*.

DIP- δ hairpin oligos (CAPS represent gene-specific sequences):
ctagcagtGACGATAAGAAACCTACAATAtagttatattcaag-cataTTGTAGGTTTCTTATCGTCAGcg.
aattcgcCTGACGATAAGAAACCTACAAtat-gcttgaatataactaTATTGTAGGTTTCTTATCGTCactg.

UAS-DIP- δ RNAi plasmid was injected into the attp40 landing site, using Φ C31 integration (BestGene).

Generation of DIP- $\delta^{T2A-Gal4}$

DIP- $\delta^{T2A-Gal4}$ was generated as described in Diao *et al* (2015). In brief, flies carrying the MiMIC^{M108287} insertion were crossed with flies bearing the triplet donor cassettes (Trojan Gal4 cassettes of the three reading frames). Males from this progeny carrying both components were crossed to females carrying germline transgenic sources of Cre and Φ C31. Adult progeny with all relevant components were crossed to UAS-GFP balanced on the 3rd chromosome. Single males from this final cross were screened by fluorescence microscopy for Gal4 expression.

Generation of QF2 driver

To generate the R71G10-QF2 driver, the QF2 sequence was amplified from pattB-DSCP_prom-QF7-hsp70_term (a gift from Chris potter) using the QF-F and QF-R primers, and cloned into pBPGUw plasmid, using the Gibson assembly kit (NEB) to create pBPGUw-QF2. Then, the GMR71G10 entry vector (Alyagor *et al*, 2018) was recombined into pBPGUw-QF2 using LR recombinase (Invitrogen). Finally, the DSCP promoter region within the GMR71G10-QF2 was replaced with hsp70 promoter by RF cloning using the hspF and hspR primers. The GMR71G10-QF2^{hsp70} plasmid was injected into the attp40 landing site, using Φ C31 integration (BestGene).

QF-F TAAGCCAACCTTTGAATCACAAGACGCATACCAAACGGTA
CATGCCACCCAAG

QF-R
TGAATAATTTTCTATTTGGCTTTAGTCGACGGTATCGATAATCA
CTGTTCGT

HspF
AAGTGGTGATAAACGGCCGCGGAGCGCCGAGTATAAATAG
AG

HspR
AAGTGGTGATAAACGGCCGCGGAGCGCCGAGTATAAATAG
AG

Generation of MARCM clones

Due to centromeric chromosomal location of dpr12, we could not generate dpr12 mutant clones and instead expressed dpr12-RNAi within γ -KC clones. MB γ -KC MARCM clones were generated as described in Lee and Luo (1999). In brief, flies were heat shocked (hs) for 40–60 min at 37°C at 24 h after egg laying and examined at the indicated developmental time points.

To discover the mitotic window which results in adult PAM-DANs, we used the MARCM technique to generate DIP- $\delta^{T2A-Gal4}$

clones by hs at different developmental times. Only hs at 0–24 h after egg laying resulted in clones containing PAM-DANs, and therefore, this hs regime was used in this study. Importantly, here mitotic recombination was performed using FRT40A and used to eliminate Gal80 expression but *DIP- δ* remained heterozygous as it is on another chromosome.

Immunostaining and imaging

Brains were dissected in ringer solution, fixed using 4% paraformaldehyde (PFA) for 20 min at room temperature (RT), and washed with PB with 0.3% Triton-X (PBT, three immediate washes followed by 3 \times 20 min washes). Non-specific staining was blocked using 5% heat inactivated goat serum in PBT and then samples were subjected to primary antibodies (over-night, 4°C) and secondary antibodies (2 h at RT) with PBT washes (three quick washed followed by 3 \times 20 min washes). The brains were mounted on SlowFade (Invitrogen) and imaged using Zeiss LSM800 confocal microscope. Images were processed with ImageJ 1.51 (NIH). Individual neurons were traced manually through all focal planes using the Edge Detection Settings of the Analyze Paint Brush VVD selection tool (Takashi Kawase). Thresholding was individually adapted for each focal plane and neuronal structures and refined through the Analyze Erase tool whenever necessary.

For Brp staining, brains were blocked in 2% bovine serum albumin (BSA) in PBT for 2 h at RT, incubated with mouse anti-Brp antibody for two days at 4°C, and then incubated with secondary antibody for an over-night at 4°C. Next, brains were transferred to a poly-L-lysine (Sigma-Aldrich. # P1524-25MG) pre-treated cover glasses (22 \times 22 \times 1; Fisher Scientific. # 12-542B), fixed, dehydrated in ascending alcohol series (30%, 50%, 75%, 95%, and 3 \times 100%, 10 min each), incubated in Xylene 2 \times 10 min and embedded in DPX (Electron Microscopy Sciences; # 180627-05) and incubated for at least 4 days. Confocal laser scanning microscopy was done using an Olympus microscope equipped with a Plan-Apochromat 20x objective. Taken images were analyzed using VVD Viewer (Takashi Kawase).

Generation of EM-based models

We screened the publicly available connectome *neuPrint* 1.1 EM dataset (Clements *et al*, 2020) at the Howard Hughes Medical Institute (HHMI) Janelia Research Campus (<https://NeuPrint.janelia.org/>) for intrinsic and extrinsic MB circuit entities projecting to the γ 4 and γ 5 zones of the MB (Scheffer *et al*, 2020). The resulting EM skeletons were projected with VVD Viewer 1.1 onto the JRC2018_UNISEX template brain (Bogovic *et al*, 2020). See Appendix Table S1 for the full list of EM skeletons used.

Quantification and statistical analysis

In all cases, statistical significance was calculated as follows: *** represents a *P*-value lower than 0.001, ** represents a *P*-value lower than 0.01, and * represents a *P*-value lower than 0.05. Specific *P*-values and sample sizes are indicated in the relevant figure legends.

For quantification of regrowth (Figs 1, 4 and 8), confocal Z-stacks were given to an independent laboratory member who blindly ranked the severity of the regrowth defects. For statistical analysis, Kruskal–Wallis test was performed followed by a Wilcoxon–Mann–Whitney test.

Data availability

The RNA-seq data have been deposited in NCBI's Gene Expression Omnibus and are accessible through GEO series accession number GEO: GSE165896 (<https://www.ncbi.nlm.nih.gov/geo/query/acc.cgi?acc=GSE165896>).

Expanded View for this article is available online.

Acknowledgements

We thank Larry Zipursky and Brian McCabe for sharing reagents and the Bloomington Stock Centers for reagents; monoclonal antibodies were obtained from the Developmental Studies Hybridoma Bank developed under the auspices of the NICHD and maintained by the University of Iowa. We thank R. Rothkopf for assistance with statistics; M. Schuldiner, A. Yaron, T. Misgeld, and the O.S laboratory for discussions and critical reading of this manuscript. We thank Life Science Editors for editing assistance. Funding: This work was supported by the European Research Council (erc), consolidator grant # 615906, "AxonGrowth", the Volkswagen Stiftung (joint Lower Saxony–Israel) grant # ZN3459, the Sagol Institute for Longevity Research, and the Deutsche Forschungsgemeinschaft (DFG) grant RI 2419/4-1. Fly food for this project was funded by the Women Health Research Center. O.S. is the Incumbent of the Prof. Erwin Netter Professorial Chair of Cell Biology, T.R. was supported by Axa as team member of the Axa Chair from genome to structure, and F.R. is a GSF member and was supported by Evangelisches Studienwerk Villigst e.V.

Author contributions

BB designed, performed, and analyzed experiments, performed bioinformatic analyses, and wrote the manuscript. HM designed, performed, and analyzed experiments and wrote the revised manuscript. RA designed, performed, and analyzed experiments. IA designed and performed the RNA-seq experiments and performed bioinformatic analyses. VB, GC, and FR performed specific experiments. HK-S performed and analyzed the RNA-seq experiments. ED performed bioinformatic analyses. TM performed image analyses and provided important conceptual insights. OS led the project, designed experiments, interpreted results, and wrote the manuscript.

Conflict of interest

The authors declare that they have no conflict of interest.

References

- Alyagor I, Berkun V, Keren-Shaul H, Marmor-Kollet N, David E, Mayselless O, Issman-Zecharya N, Amit I, Schuldiner O (2018) Combining developmental and perturbation-seq uncovers transcriptional modules orchestrating neuronal remodeling. *Dev Cell* 47: 38–52
- Ashley J, Sorrentino V, Lobb-Rabe M, Nagarkar-Jaiswal S, Tan L, Xu S, Xiao Q, Zinn K, Carrillo RA (2019) Transsynaptic interactions between IgSF proteins DIP-alpha and Dpr10 are required for motor neuron targeting specificity. *eLife* 8: e42690
- Aso Y, Hattori D, Yu Y, Johnston RM, Iyer NA, Ngo TT, Dionne H, Abbott LF, Axel R, Tanimoto H *et al* (2014a) The neuronal architecture of the mushroom body provides a logic for associative learning. *eLife* 3: e04577
- Aso Y, Sitaraman D, Ichinose T, Kaun KR, Vogt K, Belliart-Guerin G, Placais PY, Robie AA, Yamagata N, Schnaitmann C *et al* (2014b) Mushroom body output neurons encode valence and guide memory-based action selection in *Drosophila*. *eLife* 3: e04580

- Aso Y, Ray RP, Long X, Bushey D, Cichewicz K, Ngo TT, Sharp B, Christoforou C, Hu A, Lemire AL et al (2019) Nitric oxide acts as a cotransmitter in a subset of dopaminergic neurons to diversify memory dynamics. *eLife* 8: e49257
- Beck ES, Gasque G, Imlach WL, Jiao W, Jiwon Choi B, Wu PS, Kraushar ML, McCabe BD (2012) Regulation of Fasciclin II and synaptic terminal development by the splicing factor beag. *J Neurosci* 32: 7058–7073
- Bilz F, Geurten BRH, Hancock CE, Widmann A, Fiala A (2020) Visualization of a distributed synaptic memory code in the *Drosophila* brain. *Neuron* 106: 963–976
- Bogovic JA, Otsuna H, Heinrich L, Ito M, Jeter J, Meissner G, Nern A, Colonell J, Malkesman O, Ito K et al (2020) An unbiased template of the *Drosophila* brain and ventral nerve cord. *PLoS One* 15: e0236495
- Bornstein B, Zahavi EE, Gelley S, Zosman M, Yaniv SP, Fuchs O, Porat Z, Perlson E, Schuldiner O (2015) Developmental axon pruning requires destabilization of cell adhesion by JNK signaling. *Neuron* 88: 926–940
- Carrillo RA, Ozkan E, Menon KP, Nagarkar-Jaiswal S, Lee PT, Jeon M, Birnbaum ME, Bellen HJ, Garcia KC, Zinn K (2015) Control of synaptic connectivity by a network of *Drosophila* IgSF cell surface proteins. *Cell* 163: 1770–1782
- Cheng S, Ashley J, Kurlito JD, Lobb-Rabe M, Park YJ, Carrillo RA, Ozkan E (2019) Molecular basis of synaptic specificity by immunoglobulin superfamily receptors in *Drosophila*. *eLife* 8: e41028
- Clements J, Dolafi T, Umayam L, Neubarth NL, Scheffer LK, Plaza SM (2020) neuPrint: analysis tools for EM connectomics. *bioRxiv* <https://doi.org/10.1101/2020.01.16.909465> [PREPRINT]
- Cognigni P, Felsenberg J, Waddell S (2018) Do the right thing: neural network mechanisms of memory formation, expression and update in *Drosophila*. *Curr Opin Neurobiol* 49: 51–58
- Cohn R, Morantte I, Ruta V (2015) Coordinated and compartmentalized neuromodulation shapes sensory processing in *Drosophila*. *Cell* 163: 1742–1755
- Cosmanescu F, Katsamba PS, Sergeeva AP, Ahlsen G, Patel SD, Brewer JJ, Tan L, Xu S, Xiao Q, Nagarkar-Jaiswal S et al (2018) Neuron-subtype-specific expression, interaction affinities, and specificity determinants of DIP/Dpr cell recognition proteins. *Neuron* 100: 1385–1400
- Crittenden JR, Skoulakis EM, Han KA, Kalderon D, Davis RL (1998) Tripartite mushroom body architecture revealed by antigenic markers. *Learning & Memory* 5: 38–51
- Croset V, Treiber CD, Waddell S (2018) Cellular diversity in the *Drosophila* midbrain revealed by single-cell transcriptomics. *eLife* 7: e34550
- Diao F, Ironfield H, Luan H, Diao F, Shropshire WC, Ewer J, Marr E, Potter CJ, Landgraf M, White BH (2015) Plug-and-play genetic access to *Drosophila* cell types using exchangeable exon cassettes. *Cell Rep* 10: 1410–1421
- Fiala A (2007) Olfaction and olfactory learning in *Drosophila*: recent progress. *Curr Opin Neurobiol* 17: 720–726
- Gerber B, Scherer S, Neuser K, Michels B, Hendel T, Stocker RF, Heisenberg M (2004) Visual learning in individually assayed *Drosophila* larvae. *J Exp Biol* 207: 179–188
- Gratz SJ, Ukken FP, Rubinstein CD, Thiede G, Donohue LK, Cummings AM, O'Connor-Giles KM (2014) Highly specific and efficient CRISPR/Cas9-catalyzed homology directed repair in *Drosophila*. *Genetics* 196: 961–971
- Heinz S, Benner C, Spann N, Bertolino E, Lin YC, Laslo P, Cheng JX, Murre C, Singh H, Glass CK (2010) Simple combinations of lineage-determining transcription factors prime cis-regulatory elements required for macrophage and B cell identities. *Mol Cell* 38: 576–589
- Heisenberg M (2003) Mushroom body memoir: from maps to models. *Nat Rev Neurosci* 4: 266–275
- Kim D, Langmead B, Salzberg SL (2015) HISAT: a fast spliced aligner with low memory requirements. *Nat Methods* 12: 357–360
- Kurusu M, Awasaki T, Masuda-Nakagawa LM, Kawauchi H, Ito K, Furukubo-Tokunaga K (2002) Embryonic and larval development of the *Drosophila* mushroom bodies: concentric layer subdivisions and the role of fasciclin II. *Development* 129: 409–419
- Lee T, Lee A, Luo L (1999) Development of the *Drosophila* mushroom bodies: sequential generation of three distinct types of neurons from a neuroblast. *Development* 126: 4065–4076
- Lee T, Luo L (1999) Mosaic analysis with a repressible cell marker for studies of gene function in neuronal morphogenesis. *Neuron* 22: 451–461
- Lee T, Marticke S, Sung C, Robinow S, Luo L (2000) Cell-autonomous requirement of the USP/EcR-B ecdysone receptor for mushroom body neuronal remodeling in *Drosophila*. *Neuron* 28: 807–818
- Li F, Lindsey J, Marin EC, Otto N, Dreher M, Dempsey G, Stark I, Bates AS, Pleijzier MW, Schlegel P et al (2020) The connectome of the adult *Drosophila* mushroom body: implications for function. *bioRxiv* <https://doi.org/10.1101/2020.08.29.273276> [PREPRINT]
- Love MI, Huber W, Anders S (2014) Moderated estimation of fold change and dispersion for RNA-seq data with DESeq2. *Genome Biol* 15: 550
- Lyne R, Smith R, Rutherford K, Wakeling M, Varley A, Guillier F, Janssens H, Ji W, McLaren P, North P et al (2007) FlyMine: an integrated database for *Drosophila* and Anopheles genomics. *Genome Biol* 8: R129
- Meltzer H, Marom E, Alyagor I, Mayselless O, Berkun V, Segal-Gilboa N, Unger T, Luginbuhl D, Schuldiner O (2019) Tissue-specific (ts)CRISPR as an efficient strategy for in vivo screening in *Drosophila*. *Nat Commun* 10: 2113
- Modi MN, Shuai Y, Turner GC (2020) The *Drosophila* mushroom body: from architecture to algorithm in a learning circuit. *Annu Rev Neurosci* 43: 465–484
- Nagarkar-Jaiswal S, Lee PT, Campbell ME, Chen K, Anguiano-Zarate S, Gutierrez MC, Busby T, Lin WW, He Y, Schulze KL et al (2015) A library of MiMICs allows tagging of genes and reversible, spatial and temporal knockdown of proteins in *Drosophila*. *eLife* 4: e05338
- Otto N, Pleijzier MW, Morgan IC, Edmondson-Stait AJ, Heinz KJ, Stark I, Dempsey G, Ito M, Kapoor I, Hsu J et al (2020) Input connectivity reveals additional heterogeneity of dopaminergic reinforcement in *Drosophila*. *Curr Biol* 30: 3200–3211
- Owald D, Waddell S (2015) Olfactory learning skews mushroom body output pathways to steer behavioral choice in *Drosophila*. *Curr Opin Neurobiol* 35: 178–184
- Ozkan E, Carrillo RA, Eastman CL, Weiszmann R, Waghray D, Johnson KG, Zinn K, Celniker SE, Garcia KC (2013) An extracellular interactome of immunoglobulin and LRR proteins reveals receptor-ligand networks. *Cell* 154: 228–239
- Port F, Bullock SL (2016) Augmenting CRISPR applications in *Drosophila* with tRNA-flanked sgRNAs. *Nat Methods* 13: 852–854
- Port F, Chen HM, Lee T, Bullock SL (2014) Optimized CRISPR/Cas tools for efficient germline and somatic genome engineering in *Drosophila*. *Proc Natl Acad Sci USA* 111: E2967–E2976
- Port F, Strein C, Stricker M, Rauscher B, Heigwer F, Zhou J, Beyersdorffer C, Frei J, Hess A, Kern K et al (2020) A large-scale resource for tissue-specific CRISPR mutagenesis in *Drosophila*. *eLife* 9: e53865
- Rabinovich D, Yaniv SP, Alyagor I, Schuldiner O (2016) Nitric oxide as a switching mechanism between axon degeneration and regrowth during developmental remodeling. *Cell* 164: 170–182

- Rohwedder A, Wenz NL, Stehle B, Huser A, Yamagata N, Zlatic M, Truman JW, Tanimoto H, Saumweber T, Gerber B et al (2016) Four individually identified paired dopamine neurons signal reward in larval *Drosophila*. *Curr Biol* 26: 661–669
- Sanz R, Ferraro GB, Fournier AE (2015) IgLON cell adhesion molecules are shed from the cell surface of cortical neurons to promote neuronal growth. *J Biol Chem* 290: 4330–4342
- Saumweber T, Rohwedder A, Schleyer M, Eichler K, Chen YC, Aso Y, Cardona A, Eschbach C, Kobler O, Voigt A et al (2018) Functional architecture of reward learning in mushroom body extrinsic neurons of larval *Drosophila*. *Nat Commun* 9: 1104
- Scheffer LK, Xu CS, Januszewski M, Lu Z, Takemura SY, Hayworth KJ, Huang GB, Shinomiya K, Maitlin-Shepard J, Berg S et al (2020) A connectome and analysis of the adult *Drosophila* central brain. *eLife* 9: e57443
- Shuai Y, Hirokawa A, Ai Y, Zhang M, Li W, Zhong Y (2015) Dissecting neural pathways for forgetting in *Drosophila* olfactory aversive memory. *Proc Natl Acad Sci USA* 112: E6663–E6672
- Tan L, Zhang KX, Pecot MY, Nagarkar-Jaiswal S, Lee PT, Takemura SY, McEwen JM, Nern A, Xu S, Tadros W et al (2015) Ig superfamily ligand and receptor pairs expressed in synaptic partners in *Drosophila*. *Cell* 163: 1756–1769
- Tanaka NK, Tanimoto H, Ito K (2008) Neuronal assemblies of the *Drosophila* mushroom body. *J Comp Neurol* 508: 711–755
- Unger T, Jacobovitch Y, Dantes A, Bernheim R, Peleg Y (2010) Applications of the restriction free (RF) cloning procedure for molecular manipulations and protein expression. *J Struct Biol* 172: 34–44
- Venkatasubramanian L, Guo Z, Xu S, Tan L, Xiao Q, Nagarkar-Jaiswal S, Mann RS (2019) Stereotyped terminal axon branching of leg motor neurons mediated by IgSF proteins DIP-alpha and Dpr10. *eLife* 8: e42692
- Vert JP, Foveau N, Lajaunie C, Vandenbrouck Y (2006) An accurate and interpretable model for siRNA efficacy prediction. *BMC Bioinformatics* 7: 520
- Xu S, Xiao Q, Cosmanescu F, Sergeeva AP, Yoo J, Lin Y, Katsamba PS, Ahlsen G, Kaufman J, Linaval NT et al (2018) Interactions between the Ig-superfamily proteins DIP-alpha and Dpr6/10 regulate assembly of neural circuits. *Neuron* 100: 1369–1384.e1366
- Yaniv SP, Issman-Zecharya N, Oren-Suissa M, Podbilewicz B, Schuldiner O (2012) Axon regrowth during development and regeneration following injury share molecular mechanisms. *Curr Biol* 22: 1774–1782
- Yaniv SP, Meltzer H, Alyagor I, Schuldiner O (2020) Developmental axon regrowth and primary neuron sprouting utilize distinct actin elongation factors. *J Cell Biol* 219: e201903181
- Zinn K, Ozkan E (2017) Neural immunoglobulin superfamily interaction networks. *Curr Opin Neurobiol* 45: 99–105